MECHANICAL CHARACTERIZATION OF THIN FILM OLIGOMERIC SILSESQUIOXANE POLYMER COATED ON SILICON SUBSTRATE WITH NANOINDENTATION MEASUREMENTS

By

MUTHANNA K. KAREEM

A thesis submitted to the

School of Graduate Studies

Rutgers, The State University of New Jersey

In partial fulfillment of requirements

For the degree of

Master of Science

Graduate Program in Mechanical and Aerospace Engineering

Written under the direction of

Professor Assimina A. Pelegri

and approved by

_____

_____

_____

New Brunswick, New Jersey
January, 2018

ABSTACT OF THE THESIS

MECHANICAL CHARACTERIZATION OF THIN FILM OLIGOMERIC SILSESQUIOXANE POLYMER COATED ON SILICON SUBSTRATE WITH NANOINDENTATION MEASUREMENTS

By MUTHANNA K. KAREEM

Thesis Director:
Assimina A. Pelegri

Nanoindentation measurements were carried out using coatings of oligomeric silsesquioxane polymer (melting gel) (Tc: 150°C) deposited by blade (knife coating) technology on a silicon substrate. Consequently, the blade specimens were heated to different temperatures on a hot plate. This experimental protocol enables the study of kinetic principles pertinent to different experimental conditions and their effects on the final morphologies of melting gel films. The mechanical properties of the thin oligomeric silsesquioxane polymer film on a silicon substrate are evaluated using nanoindentation. A wide range of loads is applied by employing a Hysitron TI-750 Ubi nanoindenter. The instrument utilizes a Berkovich indenter, and during experimentation, the maximum penetration depth is limited up to 10% of the film thickness to avoid unintentional probing of the substrate properties. Load and depth control nanoindentation experiments enabled the quantitative determination of localized mechanical properties such as Young's modulus and hardness. The morphology and surface roughness of the specimens were also accounted in the result interpretation.

Acknowledgements

I would like to thank my advisor Professor Assimina A. Pelegri, for her patience, encouragement, and support throughout my graduate studies at the Mechanical and Aerospace Engineering Department at Rutgers, the State University of New Jersey, Professor Jonathan Singer for the fruitful discussion and amble help in explaining the intrinsic diffusion mechanisms I encountered in my studies, and Ms Lin Lei for all her help in preparing the specimens. In addition, I would like to thank Professor's Pelegri group which has been very helpful and especially Mr. Max Tenorio. All my thanks to my government for supporting my Master's degree in the USA. My family has and continues to support me through my whole life, making my successful studying and work possible. Finally, I would like to thank the Assistant Dean of graduate school, Alexandra Bachmann, for all her support before and after I came to Rutgers, the State University of New Jersey.

TABLE OF CONTENTS

ABSTACT OF THE THESIS ii

ACKNOWLEDGEMENTS iii

LIST OF TABLES v

LIST OF FIGURES xii

LIST OF ACRONYMS AND SYMBOLS xi

CHAPTER 1 1

INTRODUCTION 1

CHAPTER 2 4

NANOINDENTATION 4
2.1 Indentation theory 4
2.2 Oliver and Pharr's analysis 6
2.3 Berkovich indenter 9

CHAPTER 3 14

SPECIMEN FABRICATION AND CHARACTERIZATION PROCEDURE 14
3.1 Materials and processes 14
3.2 Specimen Preparation 17
3.3 Testing using the Hysitron instrument 18
3.4 Thin film characterization by nanoindentation 19
3.5 Experimentally characterized properties 21
3.6 Instrumentation for nanoindentation experiments 23

CHAPTER 4 25

RESULTS AND DISCUSSION 25
4.1 Nanoindentation of the 145^{0}C blade coated melting gel thin films on silicon substrate 30
4.2 Nanoindentation of the 175^{0}C blade coated melting gel thin films on silicon substrate 33
4.3 Nanoindentation of the 205^{0}C blade coated melting gel thin films on silicon substrate 35
4.4 Nanoindentation of the 175^{o}C blade coated melting gel thin films on silicon substrate – heat treatment in vacuum 38

4.5 Displacement control experiments for non-vacuum blade specimens 45
4.6 Load control experiments for vacuum and non- vacuum specimens 48

CHAPTER 5 50

CONCLUSIONS 50

REFERENCES 53

List of Tables

Table 4. 1: Comparisons of roughness parameters of blade coated melting gel thin film 26

Table 4. 2: Thickness of blade coated melting gel thin film 27

Table 4. 3: Experimental material properties of the blade melting gel specimens 41

List of Figures

Figure 2. 1: Schematics of Load – Displacement curve. h_{max} the maximum depth, h_c the contact depth, and h_f the final depth 5

Figure 2. 2: Oliver-Pharr analysis. h_{max} the maximum depth, hc the contact depth, and h_f the final depth 5

Figure 2. 3: Berkovich Indenter face angles 10

Figure 2. 4: ISO indentation standard loading and unloading cycles 11

Figure 2. 5: Schematic depicting the holding of loading and unloading period data at maximum load which can be used to measure creep within the specimen caused by thermal drift of the apparatus during a test, (a) schematic of nanoindentation creep and recovery test, and (b) load- displacement curve with thermal drift effect [21, 22]. 12

Figure 2. 6: Sink-in and pile-up during indentation; contact depth and contact areas as indicated on top and bottom images, respectively. 13

Figure 3. 1: Precursors used in methyl modified MG synthesis (a) methyltriethoxysilane (MTES) and (b) dimethyldiethoxysilane (DMDES).....14

Figure 3. 2: Spray and Blade Coating Methods. Electrospray instrumentation (left) to spray the melting gel on the Si substrate (spray coating), and blade equipment setup (right) to melting gel directly on the substrate [40, 41]. 16

Figure 3. 3: Melting gel before and after the consolidation temperature. Ethanol and water evaporated during the heat treatments. It is liquid before the consolidation temperature (120-170ºC).....16

Figure 3. 4: Melting gel (oligomeric silsesquioxane polymer) specimens glued on SEM pucks with CA glue.....17

Figure 3. 5: Elastic and plastic deformation in thin and thick films 20

Figure 3. 6: SEM images and schematics indicating effect of temperature on morphology of melting gel deposited by electrospray coating system for spray samples [26] 20

Figure 3. 7: Schematic of a Hysitron TI750 Ubi design with key components.....24

Figure 4. 1: Surface roughness of oligomeric silsesquioxane polymer (melting gel) blade coated specimens on silicon substrate. Hysitron Ti 750 Ubi microscopy mode 5X.....26

Figure 4. 2: Blade coated melting gel images of nanoindents using Hysitron Ti750 at depth control mode. Left images depict surface before indentation while right images showcase the indents. Notice surface roughness variation for the 3 different temperatures depicted. 29

Figure 4. 3: Force versus displacement curves at max peak load for melting gel thin film sample 145ºC (maximum depth 1000nm, maximum peak load 1099μN). 30

Figure 4. 4: Hardness H versus penetration depth hmax relationship for 145ºC melting gel thin film. Hardness decreases with increased indenter depth. 32

Figure 4. 5: Young's modulus E versus penetration depth hmax relationship for 145ºC melting gel thin film. Young's modulus decreases with increased indenter depth. 32

Figure 4. 6: Force versus displacement curves at the max peak load for 175ºC melting gel thin film (maximum depth 887nm, maximum peak load 1000μN). 33

Figure 4. 7: Hardness H versus penetration depth hmax relationship for 175ºC melting gel thin film. Hardness decreases with increased indenter depth. 34

Figure 4. 8: Young's modulus E versus penetration depth hmax relationship for 175ºC melting gel thin film. Young's modulus decreases with increased indenter depth. 34

Figure 4. 9: Force versus displacement curves at the peak load for 205oC melting gel thin film (maximum depth 287nm, maximum peak load 95μN). 35

Figure 4. 10: Hardness H versus penetration depth hmax relationship for 205ºC blade melting gel specimen. Hardness decreases with increased indentation depth. 37

Figure 4. 11: Young's modulus E versus penetration depth hmax relationship for 205ºC blade melting gel specimen. Young's modulus decreases with increased indentation depth. ……37

Figure 4. 12: Force versus displacement curves at the peak load for the 175ºC vacuum treated melting gel thin film (maximum depth 1331nm, maximum peak load 1850μN). 38

Figure 4. 13: Hardness H versus penetration depth hmax relationship for 175ºC vacuum blade melting gel specimen. Young's modulus decreases with increased indentation depth. …….40

Figure 4. 14: Young's modulus E versus penetration depth hmax relationship for 175ºC vacuum blade melting gel specimen. Young's modulus decreases with increased indentation depth.....40

Figure 4. 15: Hardness H versus penetration depth h_{max} for blade melting gel specimens. Hardness decreases with increased indentation depth. 43

Figure 4. 16: Young's modulus E versus penetration depth h_{max} blade melting gel specimens. Young's modulus decrease with increased indentation depth. 43

Figure 4. 17: Hardness H versus penetration depth h_{max} for blade, non-vacuum, melting gel specimens. Hardness decreases with increased indentation depth.....46

Figure 4. 18: Young's modulus E versus penetration depth h_{max} for blade, non-vacuum, melting gel specimens. Young's modulus decreases with increased indentation depth....46

Figure 4. 19: Hardness H versus maximum P_{max} for blade, vacuum and non-vacuum melting gel specimens. Hardness decreases with increased indentation depth. 49

Figure 4. 20: Young's modulus E versus P_{max} for blade, vacuum and non-vacuum, melting gel specimens. Young's modulus decreases with increased indentation depth. 49

List of Acronyms and Symbols

SEM	Scanning Electron Microscopy
h	penetration depth
h_m	maximum depth
h_f	fFinal depth after unloading
h_c	contact depth
P_{max}	maximum indenter force on the area
S	contact stiffness
H	hardness
E_s	elastic modulus of the specimen
E_i	elastic modulus of the indenter
E_r	reduce modulus of the specimen
d	indenter diameter
σ_y	yield strength
F_m	maximum force
a	contact radius
c	total crack depth
v	Poisson's ratio
v_i	Poisson's ratio of the indenter
t	coating thickness
α	indenter constant
μ	friction coefficient
a	crack length
C	Berkovich indenter compliance
A	contact area
D	indenter diameter
d	residual impression diameter
Θ	indenter tip angle
ε	constant depending on the indenter geometry
β	indenter ideal angle
Si	silicon
ISO	International Standardization Organization
Y	yield stress

Chapter 1

INTRODUCTION

The swift development of nanomaterials and their applications in thin film and coating technologies in electronics and other industries has led to an increased emphasis on their mechanical characterization at the nanoscale. Electrical, thermal, and mechanical properties are intrinsically coupled to the quality, mechanical performance, and functional integrity of thin films during their lifetime. In recent years, nanoindentation has been established as the standard method for evaluating hardness, elastic moduli, viscoelastic and other properties at the nanoscale. The purpose of this study is to assess the effect of two different thin film coating techniques, namely, electrospray and blade (knife) coating, on the mechanical properties of oligomeric silsesquioxane polymer (melting gel) (Tc: 150℃ using nanoindentation.

Oliver and Pharr proposed a method to determine the elastic modulus and hardness from indentation load-displacement curves of a bulk material. Since 1992, their proposed method has been employed similar to a standard procedure to perform mechanical characterization using indentation tests. The Oliver-Pharr method estimates the projected contact area between indenter tip and the specimen using the equations for the elastic contact of an arbitrary shape indenter as it indents a uniform and isotropic half-space [1-3]. Researchers utilized Oliver-Pharr method to analyze indentations performed on thin films to estimate their properties. The accuracy of this measurement depends on the film and substrate properties as well as the indentation depth as a fraction of the total film thickness. The error that may occur due to the effect of the substrate increases with increasing indentation depth and increasing of the elastic properties mismatch between the

film and the substrate [1, 3, 4]. The indentation depth must be limited to less than 10% of the thin film thickness to avoid substrate effects on film measurements [4-8]. To account for the indenter's elasticity, King developed a reduced elastic modulus formulation which nevertheless resulted in large data scattering due to an insufficient analytical treatment of the substrate effects, and was later expanded by Saha and Nix [4-6]. The film thickness in King's method was replaced by the difference between the film thickness and the instantaneous indentation depth. This modification allowed the accounting of the elastic recall during unloading from an elastic-plastic indentation using a Berkovich indenter. In this instance, the indenter was modeled as a flat-tip one (instead of a Berkovich) which led to overestimating the substrate effect at relatively deep indentation depths [7]. In the first few publications about the nanoindentation in the early 1990s, several authors tried to determine the Young modulus and hardness of (Ti, Nb) and (Ti, Al) coatings. Since then, researchers have become cognizant of the need for corrections in the post indentation analysis [8].

Nanoindentation provides accurate measurements of the continuous variation of the indentation load, P, as a function of the indentation depth, h. The loads and displacements during these tests are at the levels of few μN and few nanometers, respectively. Depth-Sensing Indentation (DSI) tests are performed by pushing a rigid indenter tip into a specimen [9]. The hardness obtained by a DSI test results from dividing the maximum applied load by the projected residual contacted area. Other more complicated models employed to determine the mechanical properties of thin film materials from indentation tests include the Hertz model, which applies classic contact equations between two materials [10]. The effect of the substrate properties on indentation results of thin films is

the most significant challenge of using the Hertz model to attain the hardness**.** More recently, techniques that probe the mechanical properties of materials on the submicron scale have been developed. These methods use specialized nanoindenters, such as the Hysitron TI 750 Ubi which has a more refined indentation head than the competing Micromaterials Inc. instruments, and can perform indentations up to 9mN (30mN with a specialty transducer.) The above-mentioned piece of equipment is used in our laboratories to determine mechanical properties even when the indentation imprints are too small to be conventionally imaged.

In this Master's thesis the nanoindentation behavior of single and few layers of oligomeric silsesquioxane thin films have mechanically characterized using a Hysitron nanoindenter.

Chapter 2

NANOINDENTATION

2.1 Indentation theory

The nanoindentation technique relates the application of controlled load (nN-μN range) by utilizing of a hard indenter tip with synchronous measurement of depth (nm-μm range) to assess material properties at the nanoscale. The resulting loading (and unloading) versus displacement curves are translated into force-indentation depth graphs from which the material properties can be calculated [1, 11]. Several researchers have studied the material properties of different material systems including polymers using different indenter tips and nanoindentation methods [12, 13]. The indenter tip geometries used in nanoindentations control the depth of imprints whose area is used to calculate the total contact area at every point of the indentation process. Thin film nanoindentations employ a variety of micro mechanistic processes that aid in the calculation of contact areas at the nanoscale [14]. Specifically, the loading curve represents the intertwined response of the material to strain including elastic, plastic, and even phase transformation deformation mechanisms (see Figures 2.1-2), while initial portion of the unloading curve is used to estimate the load/depth slope, dP/dh where P is the load and h is the indentation depth, in order to calculate the reduced elastic modulus of the material. The slope of the unloading curve is usually found by curve fitting of a fifth order polynomial for any depth smaller than 1000nm (based on specific calibrations), and a lower order polynomials for depths larger than 1000nm. In this calculation the indenter's elastic properties are included, this the reduced modulus term, nevertheless, since the material properties of the indenter are known the young's modulus of the tested material can be straightforwardly derived. The

hardness of the material can be also derived from the measured indentation depth by calculating the area of the imprint which is representative of the indenter geometry.

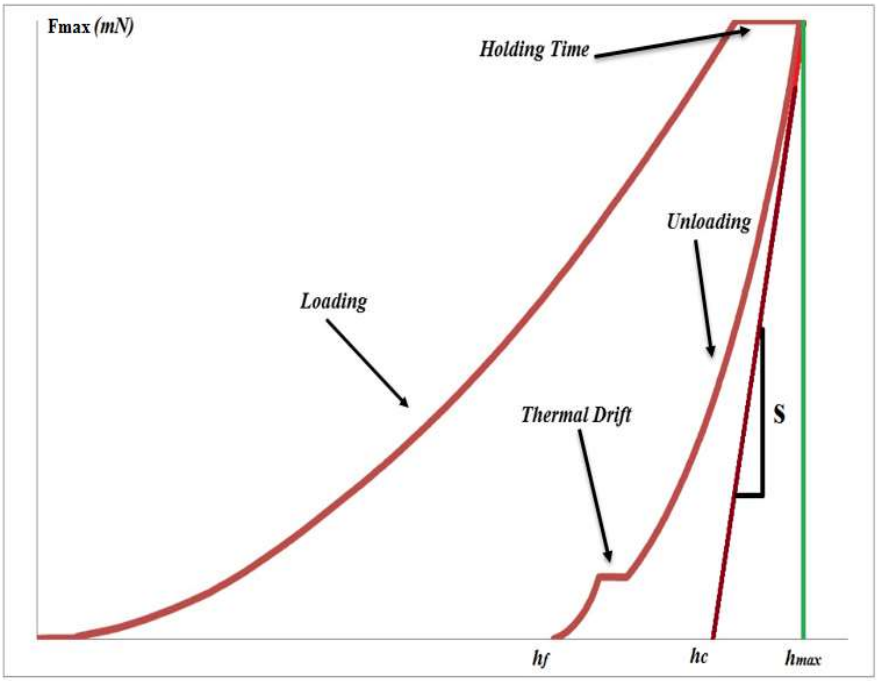

Figure 2. 1: Schematics of Load – Displacement curve. h_{max} the maximum depth, h_c the contact depth, and h_f the final depth

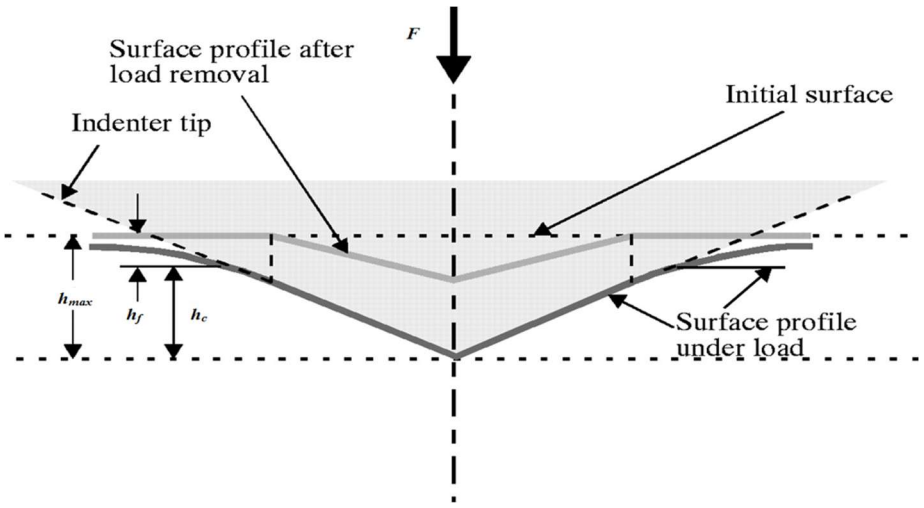

Figure 2. 2: Oliver-Pharr analysis. h_{max} the maximum depth, hc the contact depth, and h_f the final depth

2.2 Oliver and Pharr's analysis

The Oliver and Pharr method is used for determining nanoindentation load–displacement data based on the measurement of the contact stiffness. Contact stiffness is usually determined at the beginning of the unloading sequence or, when using dynamic nanoindentation, continuously during the whole loading process according to Sneddon's elastic theory[12]. Contact mechanics is essential in performing nanoindentation studies as it deals with the elastic contact and elastic-plastic contact interaction of two solid objects [14]. It enables the interpretation of the load-displacement curve and along with the other measurements derived from depth-sensing instrumentation has contributed in establishing Oliver and Pharr's work as the standard in the field [12].

The Oliver and Pharr's model describes the unloading curve measured during indentation using a power law function of the following form:

$$P = l(h - h_f)^m \tag{2. 1}$$

where h is the instantaneous indentation displacement in nm, P is the load in mN or μN, h_f is the final indentation displacement in nm, and both l and m are dimensionless proper parameters. The slope of this part of the curve is the contact stiffness of the material, S. The value of the slope represents the rate of change of loading over the rate of change of the depth, which is related to the contact area, A, and reduced modulus, E_r, as follows:

$$S = \frac{dP}{dh} = \frac{2}{\sqrt{\pi}} E_r \sqrt{A} \tag{2. 2}$$

The curve derivation yields the slope of the unloading curve. Therefore,

$$S = \frac{dP}{dh} \tag{2. 3}$$

Contact stiffness, *S*, or elastic unloading stiffness, is the value of the slope as shown in Figure 2.1 above and is used to calculate the elastic modulus at the maximum load and indentation depth of the test specimen. In contact mechanics theory, the distinction between elastic contact and elastic-plastic contact is of essence and its significance is discussed next.

2.2.1 Elastic contact

The deflections and stresses arising from the contact between two elastic solids are of particular interest to those performing indentation testing. The combination of the intender's and the specimen's elastic moduli is known as a reduced modulus (E_r) and it is calculated by equation (2. 4).

$$\frac{1}{E_r} = \frac{(1-v_i^2)}{E_i} + \frac{(1-v_s^2)}{E_s} \qquad (2.\ 4)$$

where, v_s and E_S refer to the Poisson's ratio and the elastic modulus of the specimen, respectively, while v_i and E_i refer to the Poisson's ratio and elastic modulus of the indenter. E_r can be evaluated by the applied load and the measure depth using equation (2. 5)

$$E_r = \frac{dp}{dh}\frac{1}{2h_c}\frac{1}{\beta}\sqrt{\frac{\pi}{24.5}} \qquad (2.\ 5)$$

where β =1.034 for a Berkovich indenter [14].

Using this expression, the modulus of elasticity of the specimen can be determined as long as the Poisson's ratio of the specimen is known.

2.2.2 Elastic-plastic contact

Material hardness relates to the elastic-plastic deformation during nanoindentation and has been studied by many scientists because it is a material "property" that is very sensitive to

the method used to calculate the area of indentation imprint. As such, there are many interpretations of the hardness results and the experience of the experimentalist in acquiring and interpreting the data is of paramount importance. Indentation data are interpreted as permanent deformation or penetration resistance [14] and represent the response of the contact pressure P_m on the contact area. Therefore, the hardness value of a material is calculated using the mean contact pressure and the projected contact area. The yield stress of the specimen σ_Y is directly proportional to hardness, H, and written by:

$$H = C\sigma_y \qquad \textbf{(2. 6)}$$

where $C \approx 1.5$ for materials, which have a low ratio of E/Y such as glass, while $\boldsymbol{C \approx 3}$ for materials, which have a large ratio of E/Y**.** In this study a Hysitron TI 750 Ubi nanoindenter was used, that employs a pyramidal analysis process, which produces values of h_{total} (h_{max}) and $h_{plastic}$ (h_c contact depth) along with the derived hardness and reduced modules. In this analysis, the indentation process measures the penetration depth of the calibrated diamond indenter (the function of applied load) during the loading and unloading periods [4]. The slope of the unloading curve produces the elastic and plastic properties. In order to determine the mechanical properties, a power law fit is used which is also called the Oliver Pharr method [4]. This method starts fitting at 100% maximum load and stops fitting at 20% maximum load. The power law that is applied has the form:

$$P = \alpha(h - h_c)^m \qquad (2.\ 7)$$

where α is a constant, m: is the power law index that depends on the material, and h is the penetration depth. h_c and m are constants depending on the indenter. Plastic depth is determined from

$$h_c = h_{\max} - \varepsilon(CP_{\max}) \quad (2.8)$$

where C is the contact compliance equal to the tangent at maximum load. The value of ε depends on indenter geometry, here ε is 0.75.

By using the geometry of the indenter tip, which is known, the contact projected area can be calculated indirectly. The projected contact area, A_c, for a Berkovich tip is expressed by:

$$A_c = 3\sqrt{3}h_c^{\,2}\tan\theta = 24.5h_c^{\,2} \quad \textbf{(2. 9)}$$

where $\theta = 65.3^0$ the half angle of the between two adjunct faces of the Berkovich pyramid.

2.3 Berkovich indenter

Nanoindentation studies use Berkovich indenters because the edges of the Berkovich triangular pyramid form a sharper imprint than the Vickers one and its area can be more readily calculated than a conical indenter. The face angle of the Berkovich indenter is 65.3° and its indenter tip radius is in the range of 50-100nm [12, 14]. The hardness is determined from the maximum load and the projected area:

$$H = \frac{P_{\max}}{A_c} \quad \textbf{(2. 10)}$$

The projected contact area of an ideal Berkovich indenter is given by:

$$A = 3\sqrt{3}h_c^{\,2}\tan^2\theta \quad \textbf{(2. 11)}$$

where h_c is the contact depth. For θ=65.27° (ideal Berkovich indenter) Equation 2.11 becomes:

$$A = 24.56h_c \quad \textbf{(2. 12)}$$

Then the hardness, H, is calculated by:

$$H = \frac{P}{24.56 h_c} \qquad \textbf{(2.13)}$$

The reduced elastic modules, E_r, is inversely related to the material's compliance, C, E_r=/C, *which* is obtained by analyzing the unloading curve that depends on the contact area (A):

$$C = \frac{\pi^{0.5}}{2 E_r A^{0.5}} \qquad \textbf{(2.13)}$$

In order to accurately calculate the area function we use a fifth order polynomial to fit the indentation data for up to 1000nm depth, and the second order polynomial to fit the indentation data for depths about 1000nm. Recently, ISO has issued sensing indentation testing guidelines for indentations in the nano and micro depth ranges [14]. The ISO standard 14577 refers to indentation hardness, which is evaluated by using instrumented indentation or depth sensing indentation, where the force and elastic and plastic deformations are measured (see Figure 2.3).

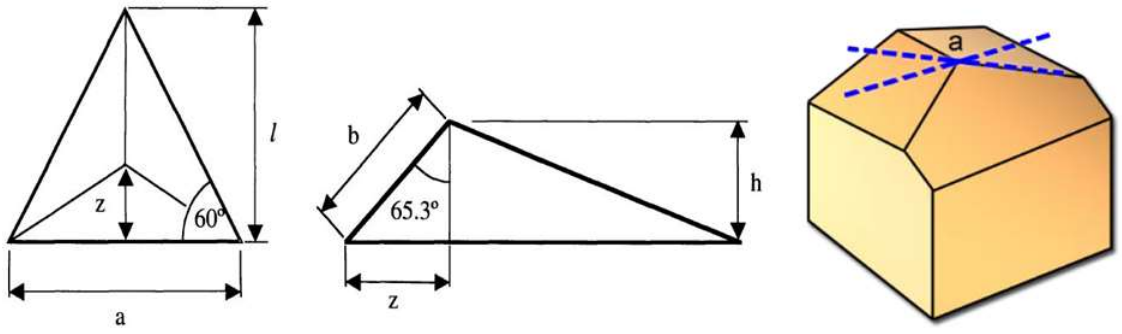

Figure 2. 3: Berkovich Indenter face angles

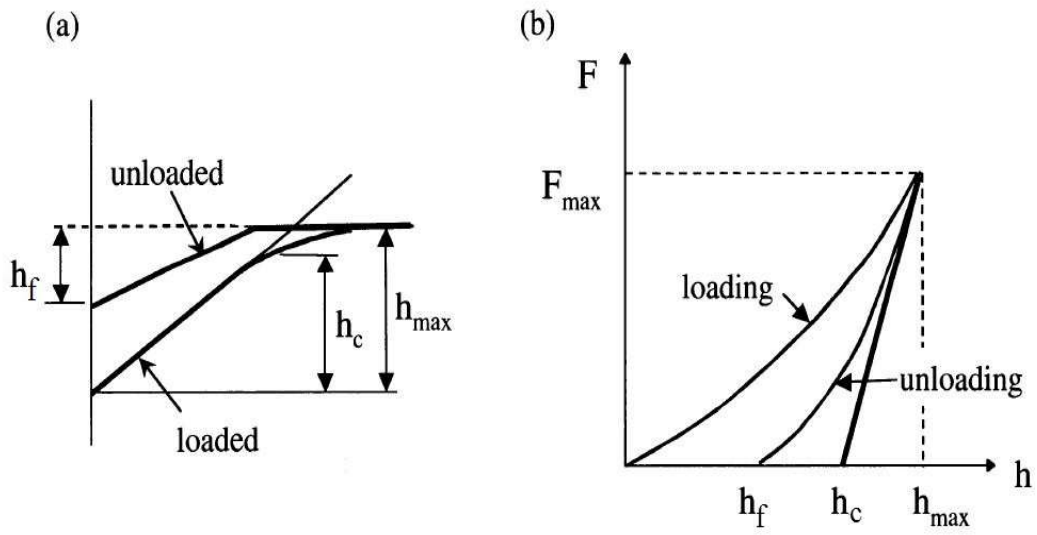

Figure 2. 4: ISO indentation standard loading and unloading cycles

2.3.1 Creep and thermal and drift

There are two types of drift behavior that has been noted. The first type is creep, which represents the plastic flow within the material while the material is subjected to constant load. That is, creep appears when the load is held constant and the depth increases as the indenter 'sinks' into the samples, see Figure 2.4. Chudoba and Richter have studied the creep influence behavior on nanoindentation measurements of hardness and elastic modulus [15].[15]. Their research indicates that the creep influence can be minimized by holding the load constant for a fixed period of time the experimentally calculated period at the maximum load which will allow to the creep to be fading.

The second type of drift is related to temperature effects. The nanoindentation thermal drift occurs when the indenter is not in thermal equilibrium. The thermal drift error is superimposed upon the depth of the real penetration depth reading. Thermal drift may cause shrinkage and thermal expansion in addition to, or alternatively, to indentation

displacement. Therefore, the testing room should be at constant environmental (temperature and humidity) conditions during testing and data acquisition to ensure accurate results. Most of the nanoindentation instruments allow for a 'hold' series of data points to accumulate, at either the end of the unloading cycle or the maximum load, to account for thermal drift correction [14, 16, 17]. The thermal drift measurement should undergo the hold period at 'unloading' because it is done at a very low load value and at that value material creep is very unlikely to occur.

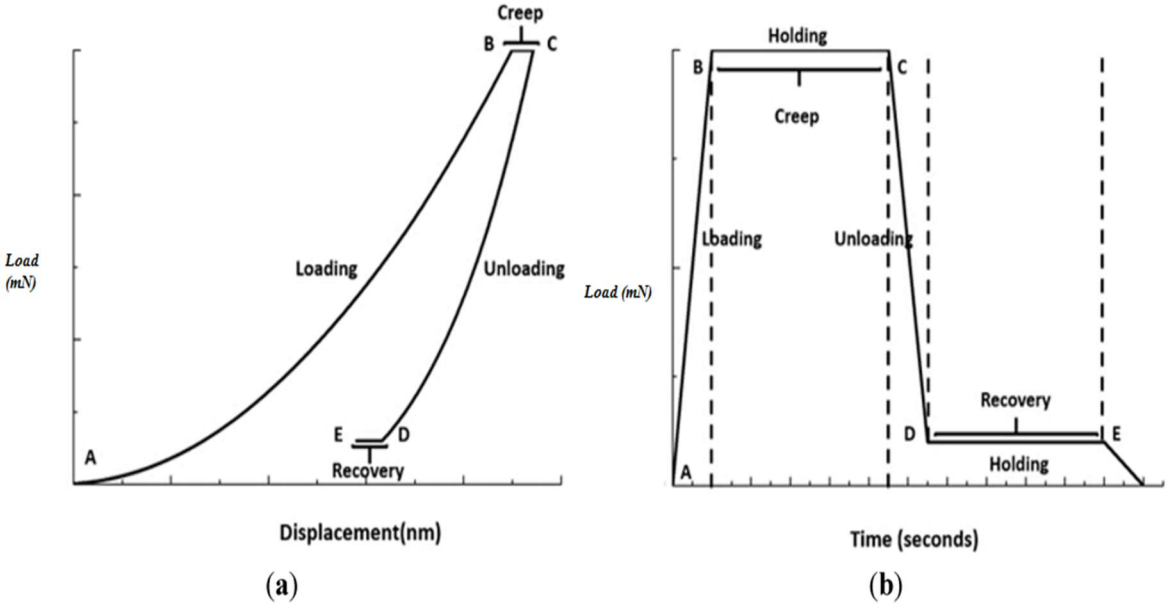

Figure 2. 5: Schematic depicting the holding of loading and unloading period data at maximum load which can be used to measure creep within the specimen caused by thermal drift of the apparatus during a test, (a) schematic of nanoindentation creep and recovery test, and (b) load- displacement curve with thermal drift effect [17, 18]. Schematic depicting the holding of loading and unloading period data at maximum load which can be used to measure creep within the specimen caused by thermal drift of the apparatus during a test, (a) schematic of nanoindentation creep and recovery test, and (b) load- displacement curve with thermal drift effect [17, 18].

2.3.2 Sinking-in and piling-up

Pile up is usually present in material systems where a soft coating is deposited on a harder substrate, such as oligomeric silsesquioxane polymer deposited on Si. Pile up can be measured using the indenter impression ratio of actual contact area (from the indenter) and corner area (from the impression). During indentation of an elastic material, the specimen surface slides inwards and under the indenter and sinking-in occurs. When the contact involves plastic deformation, the material may either sink in or pile up around the indenter, see Figure 2.5. Both sinking-in and pile-up are phenomena related to plastic deformation and their degree depends on E/Y ratio and strain hardening properties of the material [19].[19]. Most of the plastic deformations occur near the indenter, which causes the piling up. Sink-in usually occurs in materials with low *E/Y* (Young's modulus/ yield stress) ratio and little work-hardening ability. Sink-in and pile-up can affect the indentation results and overestimate the hardness as much as 60% or the elastic modulus as much as 30% [20].

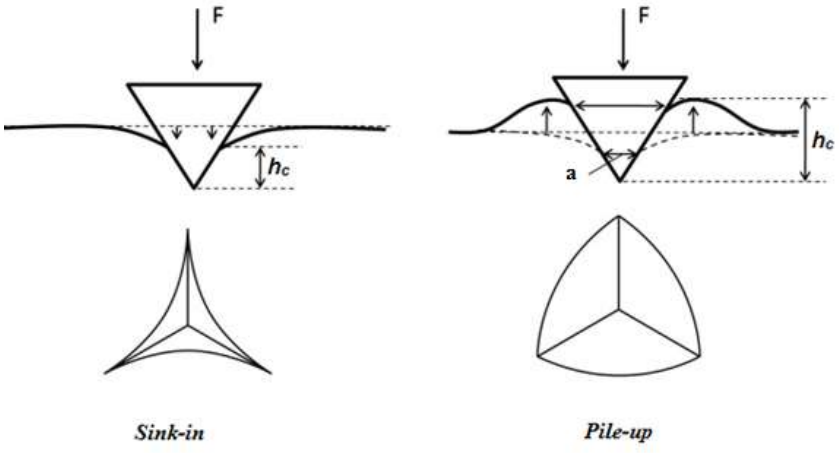

Figure 2. 6: Sink-in and pile-up during indentation; contact depth and contact areas as indicated on top and bottom images, respectively.

Chapter 3

SPECIMEN FABRICATION AND CHARACTERIZATION PROCEDURE

3.1 Materials and processes

The melting gel (MG) material used in this study was prepared using methyltriethoxysilane (MTES). The selected composition has a glass transition temperature, T_g, below temperature (-15.7°C). Above the consolidation temperature, T_c (~150°C), the MG dehydroxylates and crosslinks into irreversible hybrid organically-modified silica network.

Our specimens consist of the above melting gel (MG) thin film comprised of dimethyldiethoxysilane (DMDES) $C_{12}H_{20}O_3Si$ and methyltriethoxysilane $C_{14}H_{16}O_2Si$ [21], see Figure 3.1, and a silicon (Si) wafer as a substrate, which is regarded one of the most widely available semiconductor materials. Moreover, it is used as a substrate under coating materials in most electronic devices such as diodes, transistor, and integrated circuits.

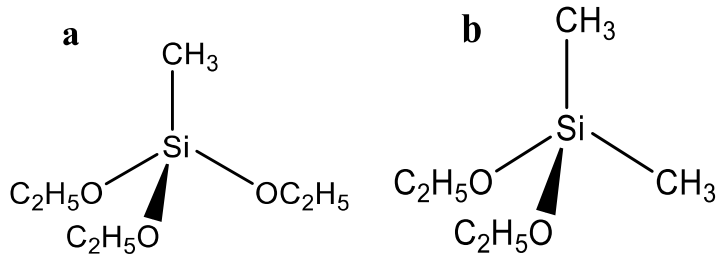

Figure 3. 1: Precursors used in methyl modified MG synthesis (a) methyltriethoxysilane (MTES) and (b) dimethyldiethoxysilane (DMDES).

The thin film coating is the oligomeric silsesquioxane polymer (MG) (Tc: 150℃) which is treated by ethanol to ensure the melting gel does not dehydrate in low temperature [22].[22]. At this temperature, the melting gel converts to organically modified silica glass

by dihydroxylation. Based on this special property, it can be processed as a viscous gel into a solid form. Parameters that affect the performance of the melting gel (MG) thin film include oxygen diffusion in the coating, processing temperature, processing time, and post coating heat treatment.

In our study we used blade coating to prepare the melting gel (MG). Blade coating is a processing method by which relative large area films are prepared on a variety of substrates, see Figure 3.2. The distance between the blade and the surface to be coated controls the thickness of the film. Other parameters that affect the quality of the thin film include coating speed, properties of substrate and film materials, surface morphology and surface energy of the substrate, and surface temperatures among others.

Professor Singer's group at Rutgers is using electrospray deposition to coat silicon wafers with this melting gel material. The goal is to fabricate coatings with designer micro/nanostructure through a large area spray or blade process. The melting gel is able to be soft (liquid) at temperatures around or less than 110^oC, but it will not stay soft at a temperature higher than 135^{o}C because of consolidation [23], see Figure 3.3.[23], see Figure 3.3. The melting gel is blade coated directly on the silicon wafer substrate, and then it is heated on a hot plate for one hour at 145^oC, 175^oC and 205^oC, separately. Note that the heat treatment temperatures are now the consolidation temperatures of these MGs.

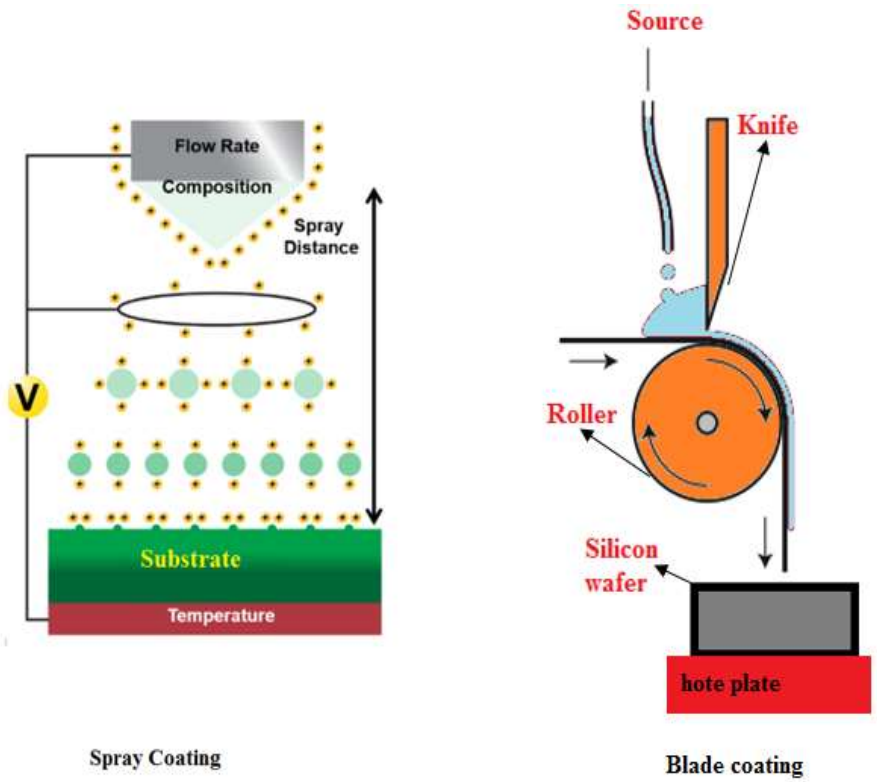

Figure 3. 2: Spray and Blade Coating Methods. Electrospray instrumentation (left) to spray the melting gel on the Si substrate (spray coating), and blade equipment setup (right) to melting gel directly on the substrate [24, 25].: Spray and Blade Coating Methods. Electrospray instrumentation (left) to spray the melting gel on the Si substrate (spray coating), and blade equipment setup (right) to melting gel directly on the substrate

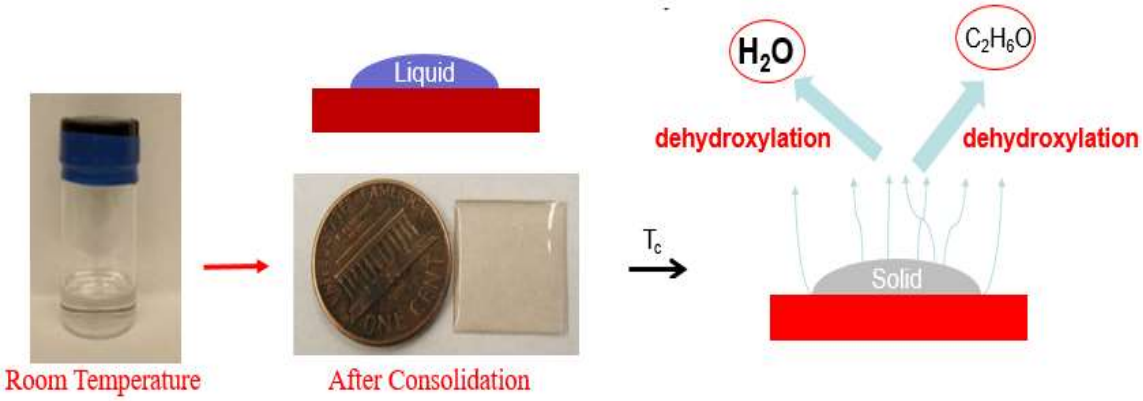

[24, 25].

Figure 3. 3: Melting gel before and after the consolidation temperature. Ethanol and water evaporated during the heat treatments. It is liquid before the consolidation temperature (150ºC).

3.2 Specimen Preparation

Due to the fabrication techniques employed in this study, there was a considerable variation in specimens' thickness. To ensure comparability and avoid substrate effects we used the data of indents up to 10% of the coating thickness for moduli and hardness characterizations. Additional load and displacement (depth) controlled experiments were performed to probe the effects of load and depth variation in the mechanical response of the films. The aforementioned experimental studies were carried out for all *145°C*, *175°C*, and *205°C* specimens.

The oligomeric silsesquioxane polymer (melting gel) (Tc: 135℃ ~ 170℃) is deposited by electrospray or blade technology on silicon wafers substrates and then glued with CA glue on SEM pucks (Figure 3. 4) to hold them in position during experimentation.

To ensure specimen fabrication reproducibility the amount of the CA glue used for each specimen was controlled and the same dosage was used for each specimen. Setting time of the glue was less than 2 mins and we allowed for a curing time of 15 mins. Furthermore, because the specimens were very thin we polished the SEM pucks with diamond paste prior to gluing them on the specimens to avoid any surface morphology effects from the puck to the silicon wafer.

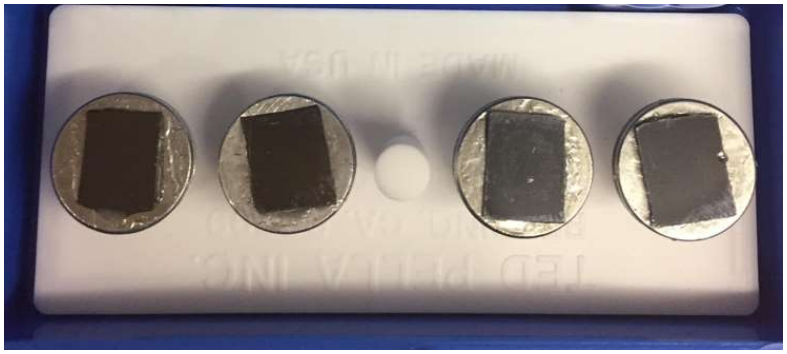

Figure 3. 4: Melting gel (oligomeric silsesquioxane polymer) specimens glued on SEM pucks with CA glue.

3.3 Testing using the Hysitron instrument

The nanoindentation experiments were performed in two instruments with complimentary load capabilities, namely, a Hysitron Ubi 750 nanoindenter with two load transducers of 9mN and 30mN capacity. The instrument uses Berkovich indenter tips for all specimens. Finally, the loading and unloading holding time is 10s for all the creep experiments.

Hysitron TI-750 Ubi nanoindenter uses a three plate capacitive transducer, which designed to allow for a high displacement sensitivity and a low thermal drift. It is preferred for measuring the mechanical properties of coatings and thin films due to its precision at low loads and it's in situ scanning probe microscopy (SPM) capabilities. SPM is particularly useful as it enables the researcher to acquire images of the specimen's surface before and after the indentation.

The specimens are prepared in Prof. Singer's laboratory and then are handed over to Prof. Pelegri's Advanced Materials and Structures laboratory, where they are characterized. Thickness determination is made at the fabrication stage and variations of thickness are reported. It is noted, that electrospraying and blade processes provide different thickness tolerances among specimens, as well as on the surface of each specimen. Again, to ensure repeatability of results we use only the 10% penetration depth thickness data for material properties characterization.

3.4 Thin film characterization by nanoindentation

Characterization of thin film properties is of paramount importance especially in industries such as aerospace, biomedical, and electronics, where multifunctional reliability and performance of these films can define the success of a product. Thin film properties differ from those of their bulk counterparts and their distinct but parallel characterization with the bulk materials can offer novel insights about their manufacturability and applications. For example, bulk materials and thin films with the same stoichiometry often vary in terms of the structure and the quality of the crystal, internal stress, and concentrations of impurities, which leads to fundamental differences in their mechanical properties.

Nanoindentation can measure the mechanical properties of thin films without removing them from the substrate. When we determine the film hardness, we must take care to avoid substrate influence. To accomplish this, the Bückle rule was developed and restricts the maximum penetration depth to 10 % of the film thickness; this guideline is usually applied to avoid any unwanted substrate influence on the measurements [5, 26].[5, 26]. Thin films should be thick enough to allow the formation of the fully developed plastic zone. This recommendation is tantamount to the mean contact pressure P_m ($P_{max} = F/A$) which is sustained at the same loading level even if the load is further increased. If the film is too thin, the plastic zone will expand to reach closer to the substrate and the results may be influenced by the substrate's properties. The most reliable and popular way to determine the hardness of a film is to perform a series of indentations at different loads, provided that the depth does not exceed 10% of the thickness of the film [27], see Figure 3.5.[27], see Figure 3.5. Another important parameter is the temperature during the film fabrication process. As seen in Figure 3.6 the morphology of the film changes depending the

processing temperature. Specifically, when the temperature is near the consolidation temperature it produces smooth thin films, while higher temperatures result in individual-droplet features because the viscous liquid doesn't have time to spray out and consolidates very fast.

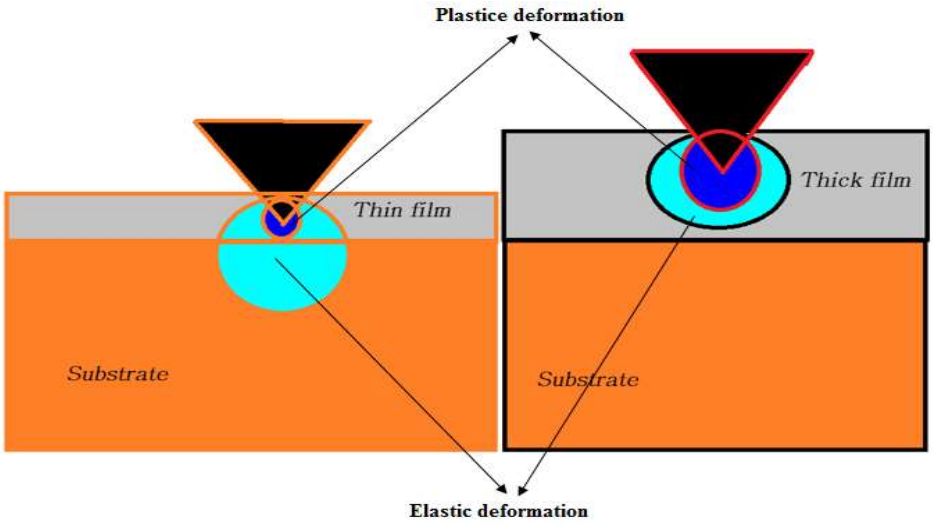

Figure 3. 5: Elastic and plastic deformation in thin and thick films

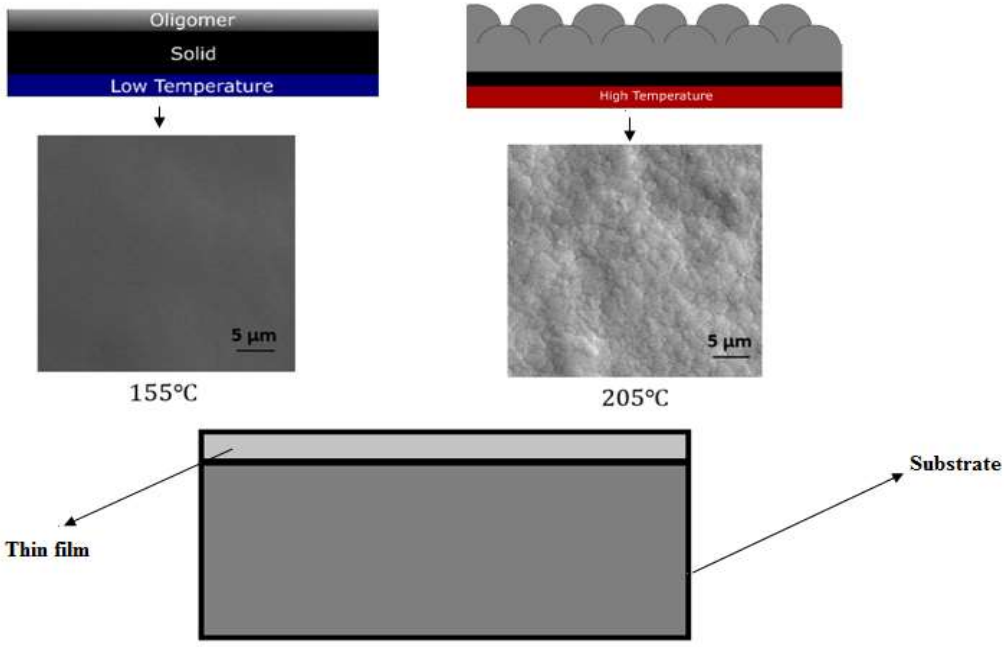

Figure 3. 6: SEM images and schematics indicating effect of temperature on morphology of melting gel deposited by electrospray coating system for spray samples [28]

3.5 Experimentally characterized properties

A material's response to applied load at the nanoscale is different than it's bulk response. For one, the surface morphology, crystallinity, and homogeneity, or absence of, becomes important as probing instrumentation and material structural intricacies are on comparable length scales. To continue, the locally developed strains and stresses do not necessarily correspond to the ones applied at the bulk structure, thus requiring material characterization at smaller scales. For this study, the hardness and the reduced modulus are the two material parameters that we will probe using nanoindentation.

3.5.1 Hardness

Hardness is usually defined in conjunction with the method used to measure it, but the most prominent definition is the measure of a solid's resistance to an applied force, usually imposed by indentation. Material hardness is typically described as a comparison between two materials, with one typically being a diamond indenter. Brinell, Vickers, Knoop, Meyer, and Martens are the most common hardness scales. We can see the imprint of the indent on the material surface which represents the extent of the plastic deformation [19]. In the Knoop and Meyer methods, the projected area is the indented area, whereas for the remaining methods the actual measured area is the indented area [29-31]. However, hardness could also be described as the resistance to abrasion, cutting, or scratching. Hardness measurements could be three main types: indentation, rebound, and scratch. In this study, indentation hardness is used as it is one of the most accurate tests. The parameters that primarily affect hardness include plasticity, elastic stiffness, strain, strength, viscoelasticity, viscosity, toughness, and ductility of the material.

3.5.2 Reduced elastic modulus

The reduced elastic modulus term signifies the effect of the indenter's properties in the measurements of a material's elastic properties at the nanoscale. Both Roa and his collaborators and Sakai's groups researched the effects of several parameters in the measurements of reduced elastic modulus and hardness of thin films, and even debated that indentations at depths less than 10% of the films' thickness should be pursued to estimate the hardness of films [30, 31]. There was a simple suggestion by Gao and his co-workers to exclude the transmission of elastic properties from film to substrate and vice versa [32]. Then, Song and Pharr modified Gao's model leading to better prediction of the substrate effect reasonably well when the film is more complaint than the substrate; this model is now called the Song and Pharr model [33-35]. This model treats the thin film under the indenter as a column allowing the film and the substrate within the column to be treated as two springs in series. Crawford and Hay modified Song and Pharr's model to consider that the substrate and the film may be in the form of parallel layers [36]. Nix and Saha further developed the nanoindentation theory [4], based on the Pharr and Oliver principle, in which the elastic modulus found easily from the indentation test by using equation (2.4). The reduced modulus (E_r) is represented in the initial output from the load-displacement curve, which is the combination of the elastic modulus of the sample and the indenter. The Berkovich tip geometry factor (β) is 1.034.

$$E_r = \frac{\sqrt{\pi}}{2\beta}\frac{S}{\sqrt{A}} \qquad \textbf{(3. 1)}$$

To calculate the elastic modulus of the sample, the Poisson's ratio of the material should be evaluated or known. Moreover, the Berkovich tip is made out of diamond with representative elastic modulus of $E_{indenter}$=1141GPa and a Poison's ratio $v_{indenter}$= 0.07 [37].

$$\frac{1}{E_r} = \frac{1-\nu^2_{sample}}{E_{sample}} + \frac{1-\nu^2_{indenter}}{E_{indenter}} \quad \textbf{(3. 2)}$$

3.6 Instrumentation for nanoindentation experiments

Researchers have used many instruments to measure the mechanical properties of the materials by applying and removing the load on the specimen, which needs to be tested. In this thesis, a Hysitron TI750 Ubi is used to evaluate the mechanical properties of thin film polymer based coatings.

The Hysitron Triboindenter®, is designed to perform indentation tests at the μN load scale (less than 25μN) [38] and nanometer depth precision to measure the mechanical properties of the materials such as hardness and elastic modulus of thin films, coatings, and bulk materials. The Hysitron can measure the load-displacement response of the nanoindentation using a three-plate capacitive transducer design providing an superior to competitors noise floor and ultra-low working force.

Our Hysitron TI 750 Ubi is able of in-situ SPM imaging by employing the same probe to scan a sample surface immediately before and/or after a test. This function allows for precise placement of the specimen as well as observation of deformation events or sample recovery after the test. The TI 750 Ubi can operate both in displacement or in load control modes giving the experimentalist total control in terms of testing mode and date acquisition Moreover, our equipment can perform in situ SPM, which is scanning probe microscopy

Imaging because the indenter tip and transducer has fixed to the piezoelectric scanner (see Figure 3.7).

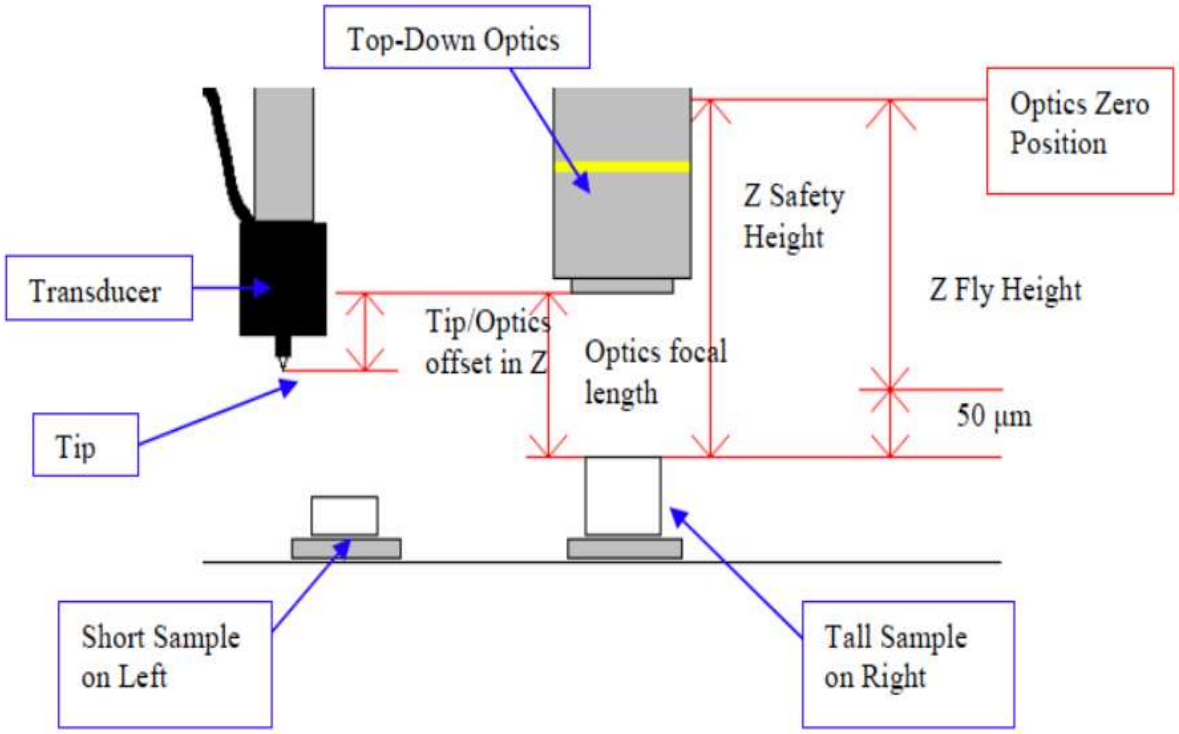

Figure 3. 7: Schematic of a Hysitron TI750 Ubi design with key components

Chapter 4

RESULTS AND DISCUSSION

In this study the melting gel blade films were made from methyltriethoxysilane (MTES) treated in ethanol solution, using silicon as a substrate material. After blade coating processing the specimens were heat treated on a hot plate for 1-hr at three different temperatures, namely, *145°C*, *175°C*, and *205°C*, which after heat treatment are designated as the consolidation temperatures of the respective MCs.

It is noted in the literature that the viscoelastic behavior of polymers changes with indentation depth; specifically the young's modulus and hardness of the polymers decreases with an increase in contact depth [9, 39-42]. In this study, results indicate that the elastic modulus and hardness are increased in low penetration depths [43-45]. The oxygen effect on the thin film melting gel will be discussed in this chapter.

The experimental results indicate that after the heat treatment of our specimens there was possible oxygen diffusion on the sample surface because the organic groups had been burned out after the consolidation temperature was reached. This leads to deterioration of the mechanical properties of the samples following heat treatments especially in the case of the specimens subjected to *205°C*, which is a temperature significantly higher than the Tc of the melting gel (oligomeric silsesquioxane polymer Tc: 150^0 C. The results demonstrate that as the spray or blade temperature is increasing from *145°C* to *205°C*, the quantities of *O-H*, CH_2 and CH_3 bonds gradually decrease, including more complete consolidation during the spray and blade coating processing. In addition,

the indentation test results exhibit that the hardness and Young's modulus decreasing with the increasing the indenter depth at high consolidation temperatures

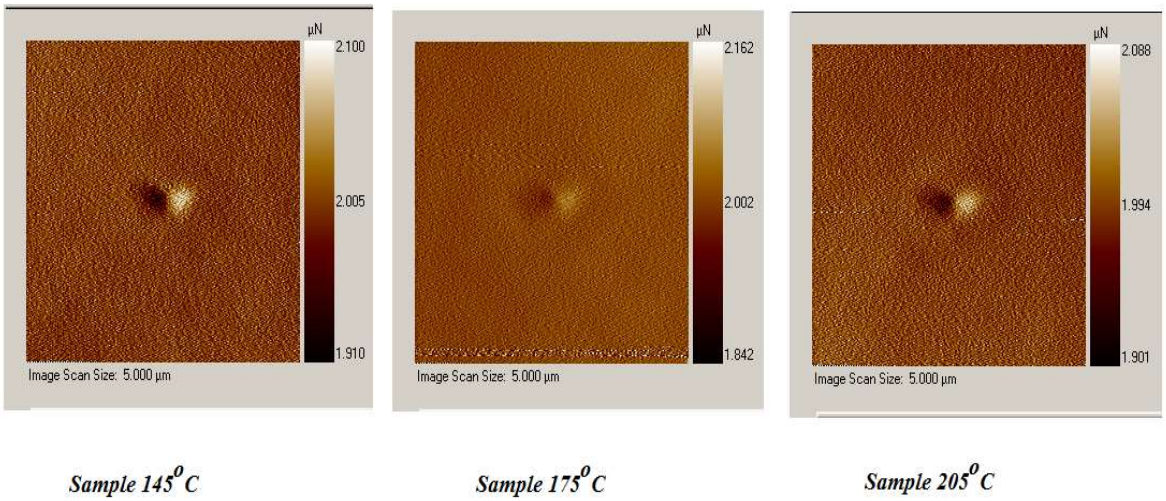

Figure 4. 1: Surface roughness of oligomeric silsesquioxane polymer (melting gel) blade coated specimens on silicon substrate. Hysitron Ti 750 Ubi microscopy mode 5X.

due to oxygen embrittlement. Also, the sample surfaces is chosen manually by using the 5X Hysitron microscopy mode (see Figure 4.1). In order to eliminate surface morphology effects, surface roughness surveys of the specimens were performed, of which the results are depicted in Table 4.1. The smoothest surfaces were selected to carry out nanoindentations.

Table 4. 1: Comparisons of roughness parameters of blade coated melting gel thin film

Sample	Scan Size	Scan rate	Average Deviation $\underline{z}$	RMS Deviation R_q	Mean Deviation R_a
145°C	$5\mu m*5\mu m$	$0.5Hz$	24.6nm	5.23nm	4.24nm
175°C	$5\mu m*5\mu m$	$0.5Hz$	26.61nm	5.40nm	4.46nm
205°C	$5\mu m*5\mu m$	$0.5Hz$	27.21nm	5.61nm	4.53nm

Table 4.1 demonstrates the roughness of measured samples as determined by AFM. No significant difference in nanoscopic roughness can be observed in these samples and all samples possess supermirror roughness as may be expected from a thermally smoothed polymeric glass.

The thickness of the melting thin films achieved with the blade coating process are tabulated in Table 4.2. As noted, there is a significantly lower thickness for the 205^0C specimens when compared to the 145^0C and 175^0C values. While all samples are nominally coated to the same thickness, dewetting from the silicon substrate occurs simultaneously with consolidation. It appears that this dewetting likely occurred to a greater extent on the higher temperature sample. Additionally, some changes in thickness may be attributed to up to 15% reduction in index of refraction that have been observed in hybrid sol-gel systems on consolidation. This change is not accounted for in the optical reflectometer measurement. It should be noted, that the vacuum designation in Table 4.2 refers to the presence of vacuum during the post-process heat treatment. As it will be later discussed, the presence of vacuum plays a role in the mechanical response of the specimens.

Table 4. 2: Thickness of blade coated melting gel thin film

Blade Spray Temperature	Minimum thickness (nm)
145ºC Non- Vacuum	10210
175ºC Non- Vacuum	9710
205ºC Non- Vacuum	2880
175ºC Vacuum	13600

Once the specimens were surveyed, nanoindentations were performed at the selected areas. The scan size was 5μm*5μm at a scanning rate of 0.5 Hz. For each site there was a pattern of 15x15 indents made spaced at 17.5μm in order to avoid pilling ups and local plastic zone effects from the neighboring indentation sites. In total 225 indents have been conducted for each specimen. Representative images of the indents for the three different types of thin film specimens per their temperature designation, ie., *145^{o}C*, *175^{o}C*, and *205^{o}C*, are illustrated in Figure, 4.2.

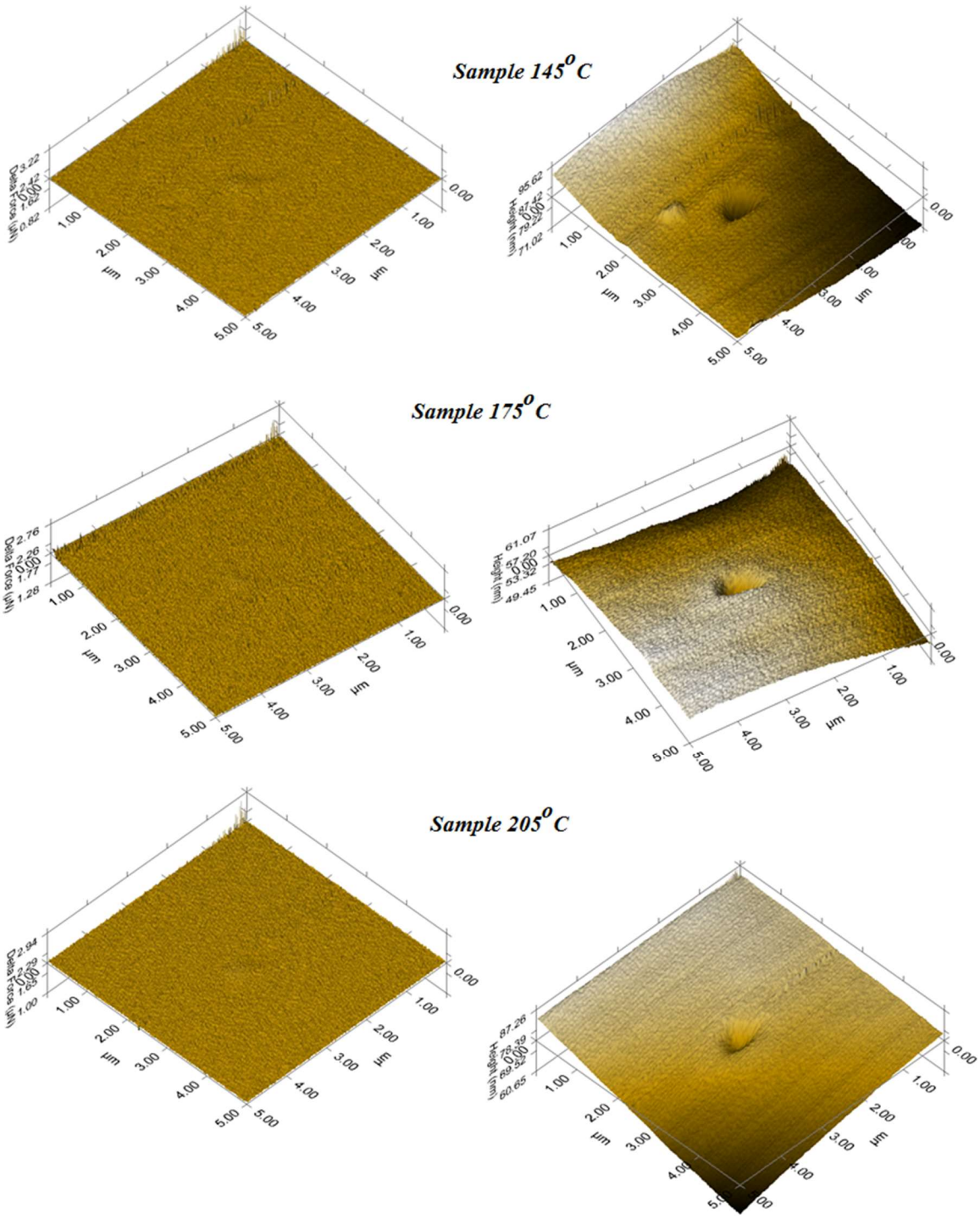

Figure 4. 2: Blade coated melting gel images of nanoindents using Hysitron TI750 at depth control mode. Left images depict surface before indentation while right images showcase the indents. Notice surface roughness variation for the 3 different temperatures depicted.

4.1 Nanoindentation of the 145^{0}C blade coated melting gel thin films on silicon substrate

The performed nanoindentation experiments on blade coated oligomeric silsesquioxane polymer (melting gel) thin films with port-processing heat treatment at *145^{0}C* are depicted in Figure 4.3. The peak load for the *145^{o}C* blade specimen is *1099.5μN* at penetration (indentation) depth of *1000nm* as is indicated in the *P vs h* plots of Figure 4.3. It should be noted that the penetration depth at the peak load is smaller than the film thickness (10210nm, Table 4.2).

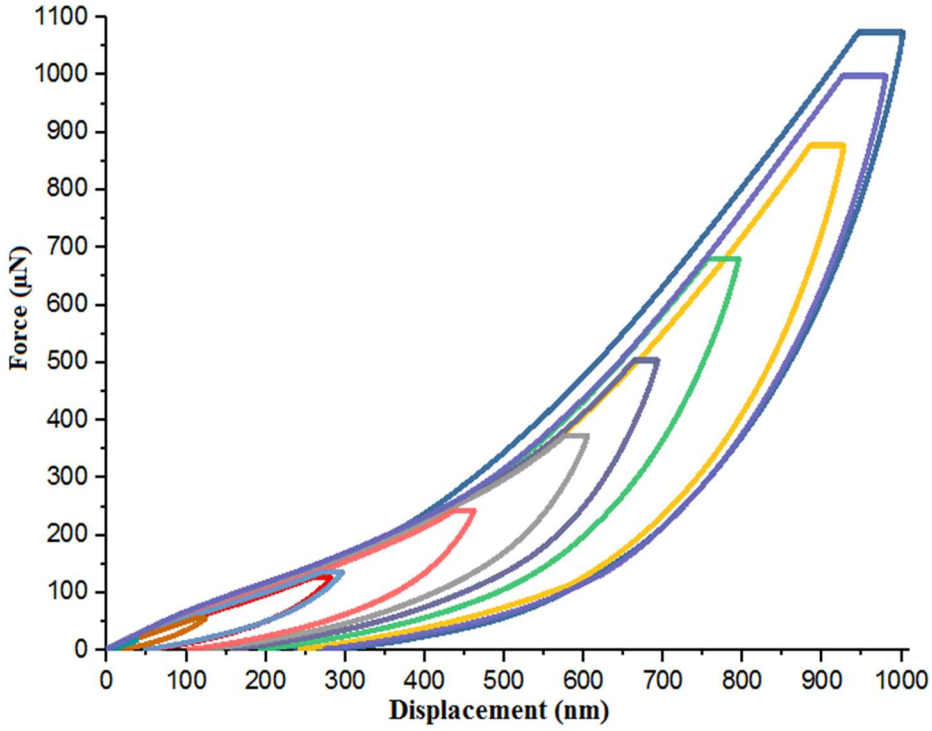

Figure 4. 3: Force versus displacement curves at max peak load for melting gel thin film sample 145^{o}C (maximum depth 1000nm, maximum peak load 1099μN).

The hardness, *H*, and Young's modulus, *E*, for each individual indent is determined using the equations provided in Chapter 2. The hardness and modulus data from the 225

indents (grid of 15x15 indents) is illustrated in the H versus h_{max} and E versus h_{max} graphs, Figures 4.4-4.5, respectively.

In order to determine the *representative* hardness and modulus values for the 145^0C specimen we use the part of the H versus h_{max} and E versus h_{max} graphs where the values of the hardness and the elastic modulus are constant, these values are in the $300 - 500nm$ range. According to the above statement, the hardness and Young's modulus for melting gel thin film 145^oC specimen is $0.061GPa$, and $0.735GPa$, respectively. Markedly, the Young's modulus and the hardness of Si wafer are referenced in the literature as $62 \sim 202GPa$ and $5.1 \sim 36.3GPa$, respectively [46].

As seen in Figures 4.4-4.5 the hardness and the Young's modulus of the melting gel thin film decreases with increased indentation depth, indicating that the thin film is harder and has higher elastic modulus closer to its free surface. That observation aligns with the accepted viscoelastic behavior of polymers, namely, decrease of their mechanical properties with increased indentation depth [47-51]. There is no manifestation of substrate effects from the Si wafer; the indentation depth at its maximum penetration does not surpass the 10% thickness of the specimen. Furthermore, any substrate effects would likely cause increase of the H and E with deeper indents since the substrate is so much stronger than the film.

In addition to the viscoelastic nature of the polymers, the MG specimens had post-processing heat treatment at 145^0C which enabled oxygen diffusion at the surface of the specimen. The oxygen reacts with the methyl-root (organic group) and burns it resulting in a stiff surface skin due to high temperature heat treatments, see Figure 4.4-4.5. This is evident in all heat treated melting gel blade samples as will be seen in the next sections.

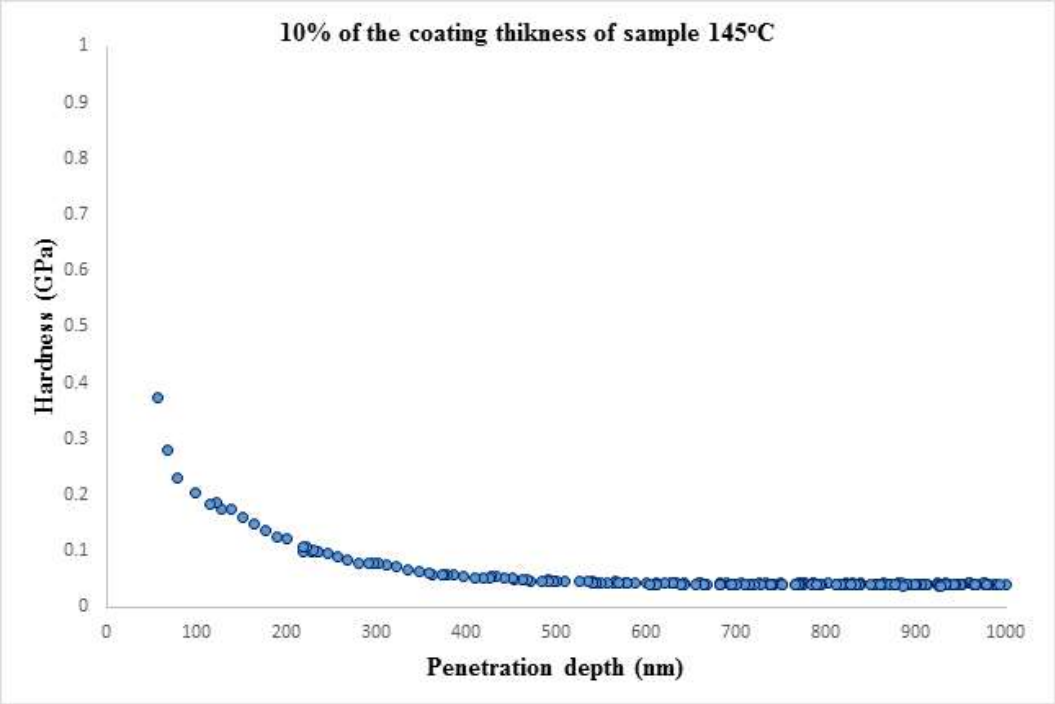

Figure 4. 4: Hardness H versus penetration depth hmax relationship for 145°C melting gel thin film. Hardness decreases with increased indenter depth.

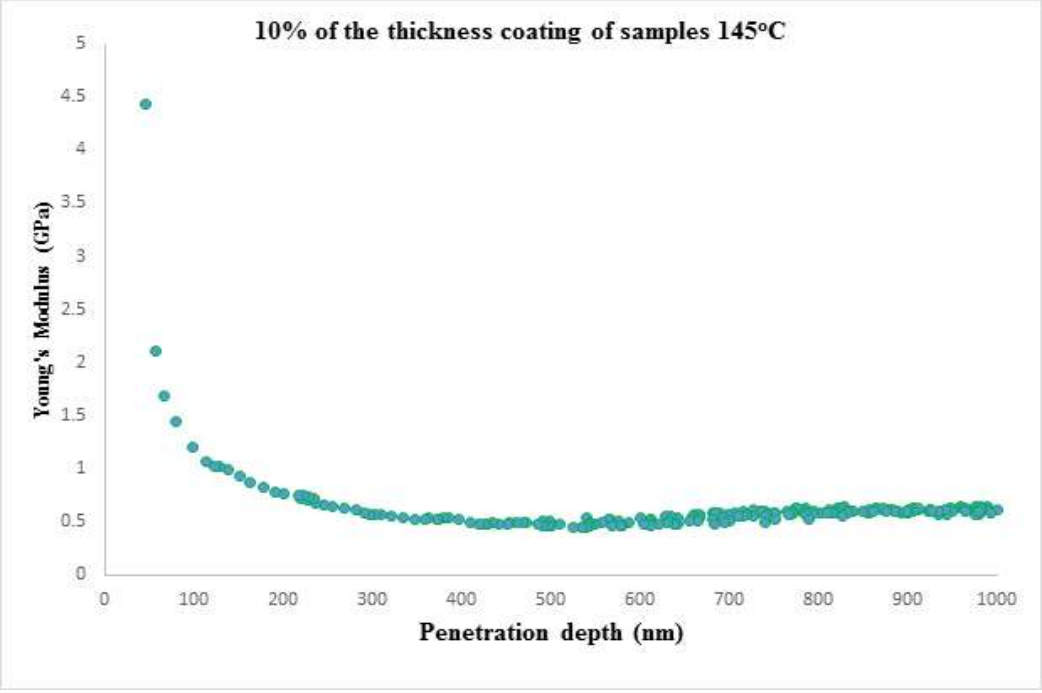

Figure 4. 5: Young's modulus E versus penetration depth hmax relationship for 145°C melting gel thin film. Young's modulus decreases with increased indenter depth.

4.2 Nanoindentation of the 175^{0}C blade coated melting gel thin films on silicon substrate

Figure 4.6 illustrates the indentations of the *175^{0}C* specimens at increasing depths until it of approximates its peak load at 10% of film thickness (9710nm in Table 4.2). The *175^{o}C* blade specimen reaches its max load value of *1000μN* at penetration (indentation) depth of *887nm* as is indicated in the *P vs h* plots of Figure 4.6.

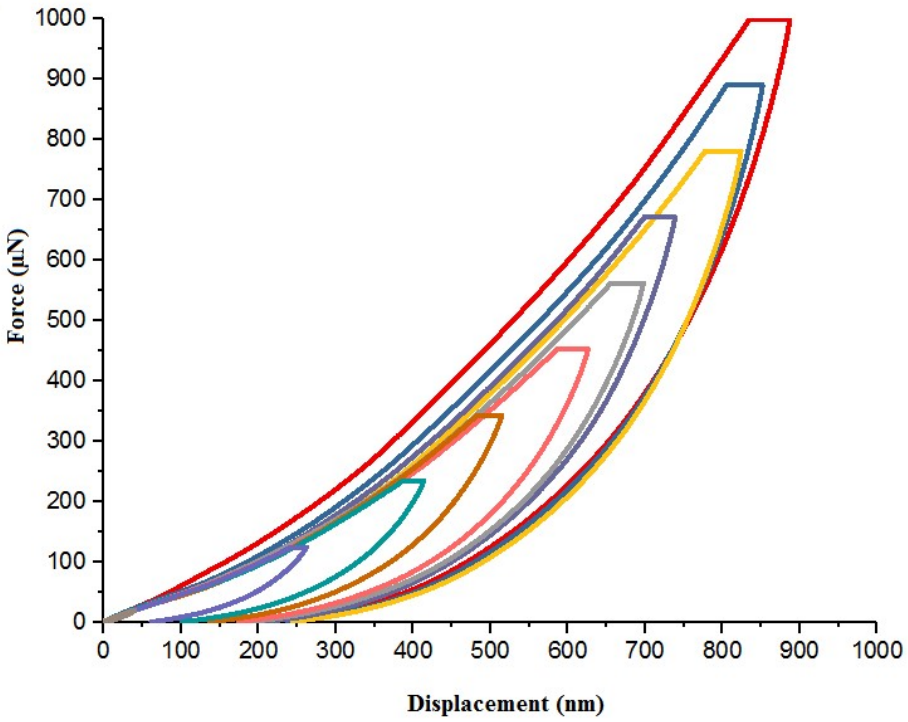

Figure 4. 6: Force versus displacement curves at the max peak load for 175ºC melting gel thin film (maximum depth 887nm, maximum peak load 1000μN).

The mechanical properties of the blade specimen heat treated at *175^{o}C* are illustrated in Figures 4.7-8. *Representative* hardness and Young's modulus are *0.098GPa*, and *0.881GPa*, respectively. These values are calculated using a data set of 225 indents (15x15 indentation grid) within the constant range of *400-900nm* of the coating's depth.

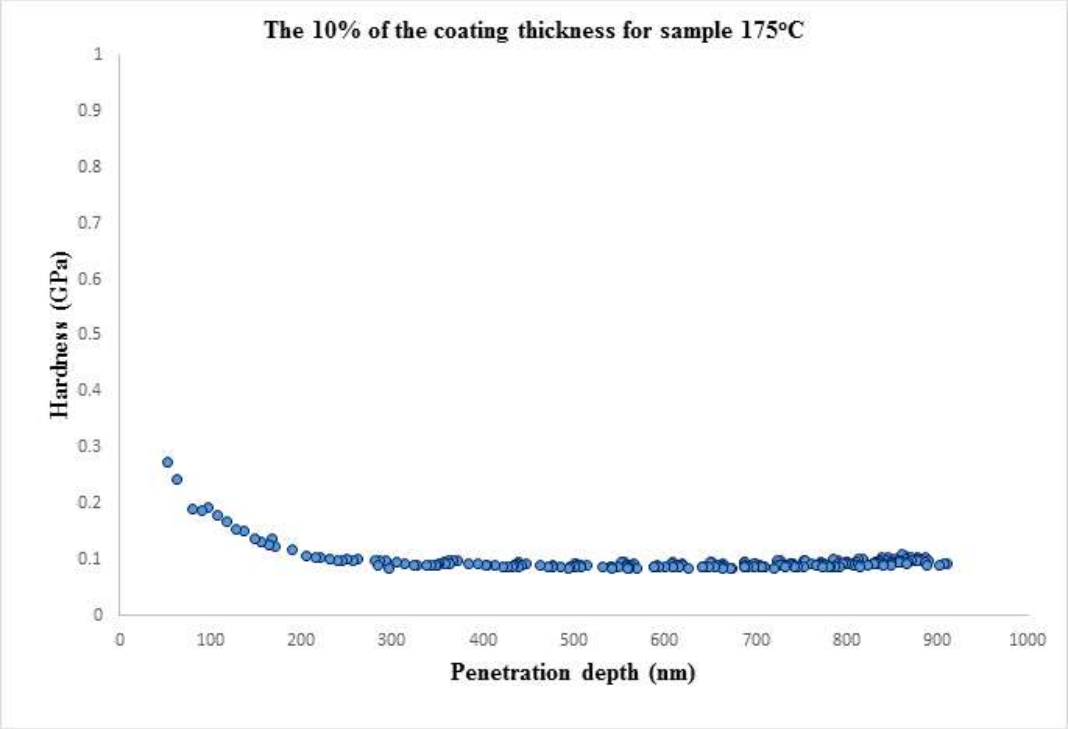

Figure 4. 7: Hardness H versus penetration depth hmax relationship for 175°C melting gel thin film. Hardness decreases with increased indenter depth.

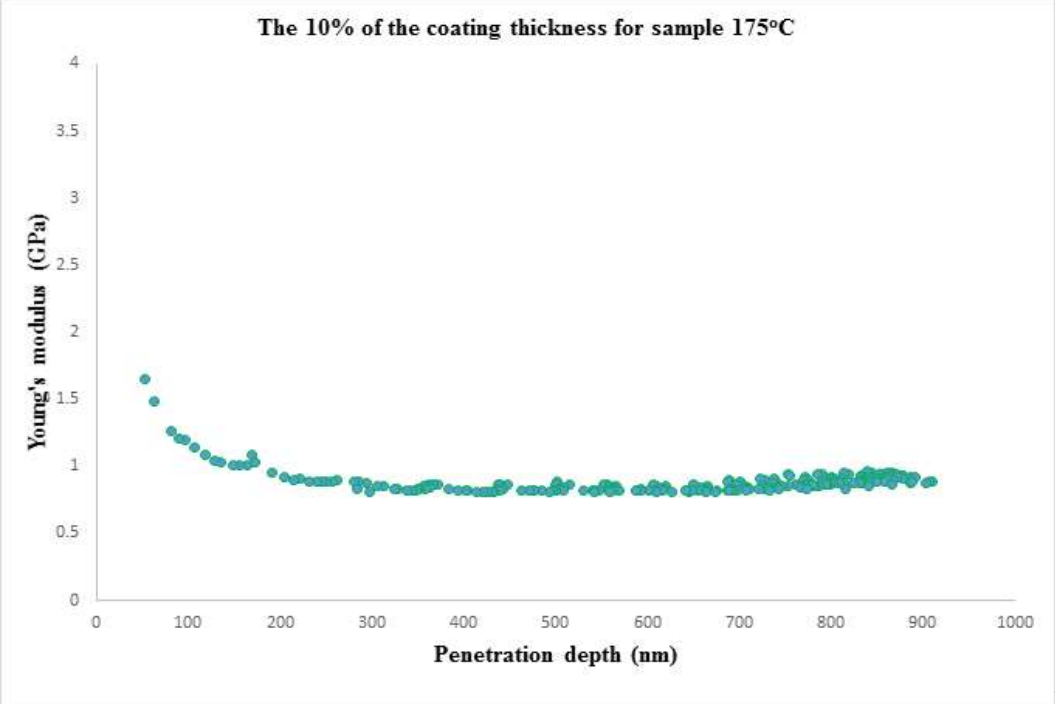

Figure 4. 8: Young's modulus E versus penetration depth hmax relationship for 175°C melting gel thin film. Young's modulus decreases with increased indenter depth.

4.3 Nanoindentation of the 205^{0}C blade coated melting gel thin films on silicon substrate

The performed nanoindentation experiments on blade coated oligomeric silsesquioxane polymer (melting gel) thin films with *205^{0}C* post processing heat treatment are illustrated in Figure 4.9. The peak load for the *205^{o}C* melting gel blade specimen is 1099.5μN at a penetration (indentation) depth of *1000nm* as it is shown in the *P vs h* plots of Figure 4.9. At the highest peak load the penetration depth is smaller than the value of 10% film thickness (2880nm, Table 4.2) ensuring the absence of substrate effects.

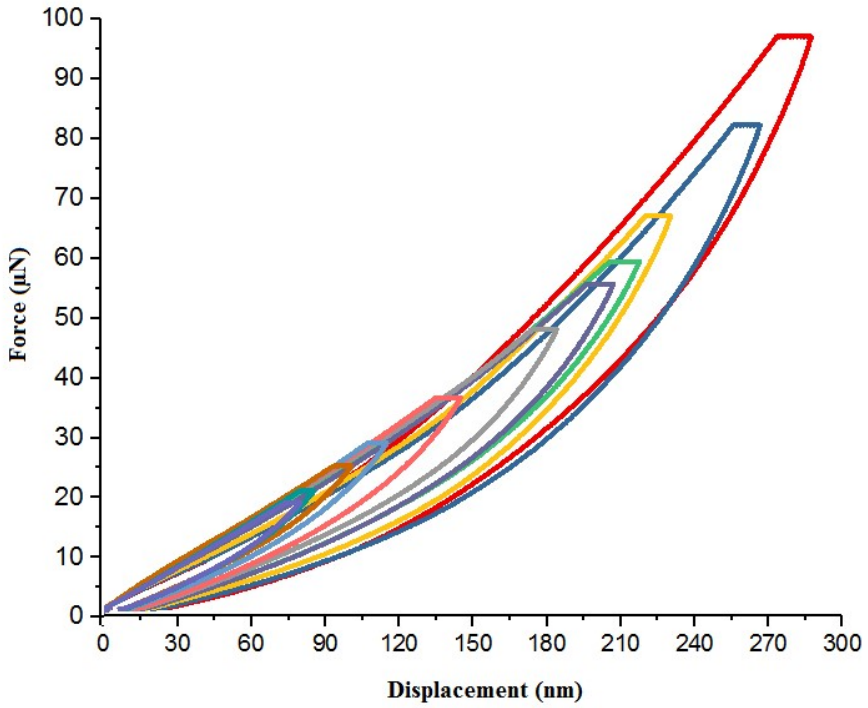

Figure 4. 9: Force versus displacement curves at the peak load for 205ºC melting gel thin film (maximum depth 287nm, maximum peak load 95μN).

The blade melting gel thin film post-processing heat treated at *205^{o}C* exhibits the lowest mechanical properties value of the three post processing heat treatments, namely *145^{o}C, 175^{o}C,* and *205^{o}C,* these are hardness of *0.041GPa* and Young's modulus of *0.56GPa*.

Figures 4.10 and 4.11 depict the H versus h_{max} and E versus h_{max} graphs for this sample and clearly illustrate the reduction in the mechanical properties when compared to the corresponding graphs for the 145^oC and 175^oC post-processing temperatures. The peak load, achieved at indentation depth close to the 10% of the film thickness, is 95μN (see Figure 4. 9), which is much lower than peak loads of the 175^0C (887nm) and 145^0C (1099.5μN).

In comparing the different processing temperatures, see Table 4.3, it is critical to recognize that there are two mechanisms at play. Above $\sim 150^oC$, the melting gel consolidates through dehydroxilation and deethyoxylation, releasing water and ethanol and converting to the hybrid gel [23, 52, 53]. This is expected to occur throughout the bulk of the gel and can therefore be considered responsible for the mechanical properties at the greatest extent of indentation. The fact that the sample consolidated at 205^oC displays reduced modulus and hardness compared to other samples is likely due to differences in the specific crosslinking that occurs during consolidation. The second process is the oxidation that occurs at the surface of the samples as the organic groups are burnt away at elevated temperatures. This causes the values of H and E to increase near the surface in all specimens, as the O-H and CH_3 bonds are removed leaving stripped silica network [54, 55].[54, 55]. This effect monotonically increases with processing temperature. Finally, the mechanical properties of the Si wafer substrate are higher than the ones of the melting gel thin film. If there were any substrate effects the H and E values of the melting film should be increasing. Thus, it is concluded that the 10% thickness indentation assumption holds for the specimens of this study.

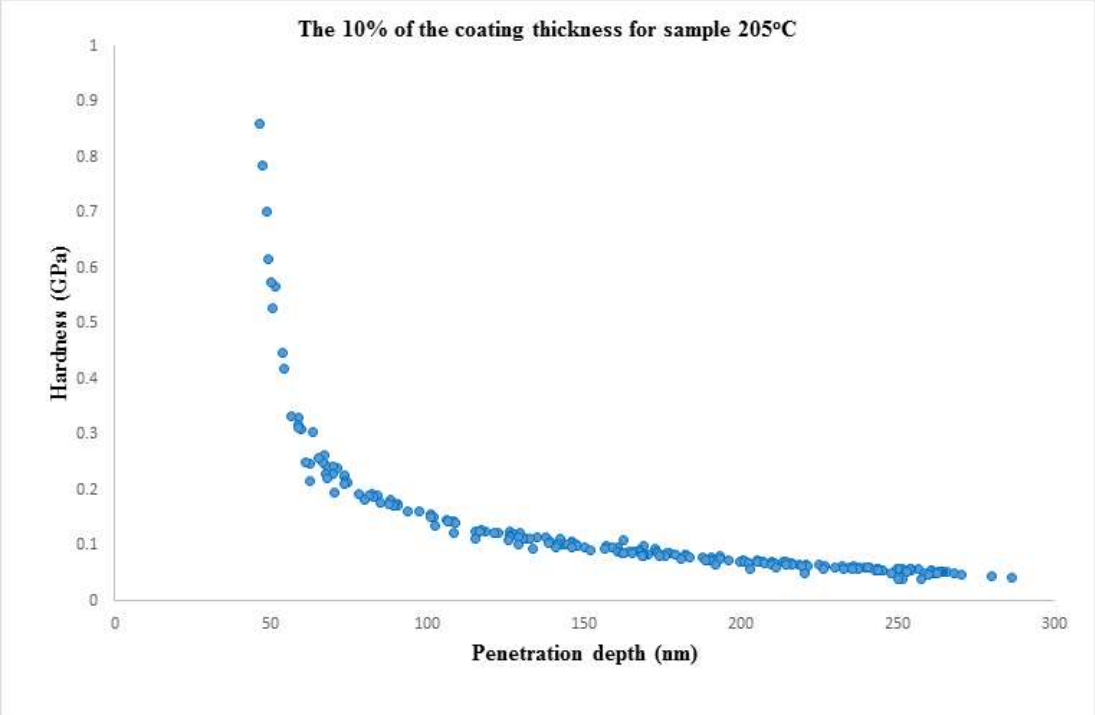

Figure 4. 10: Hardness H versus penetration depth hmax relationship for 205ºC blade melting gel specimen. Hardness decreases with increased indentation depth.

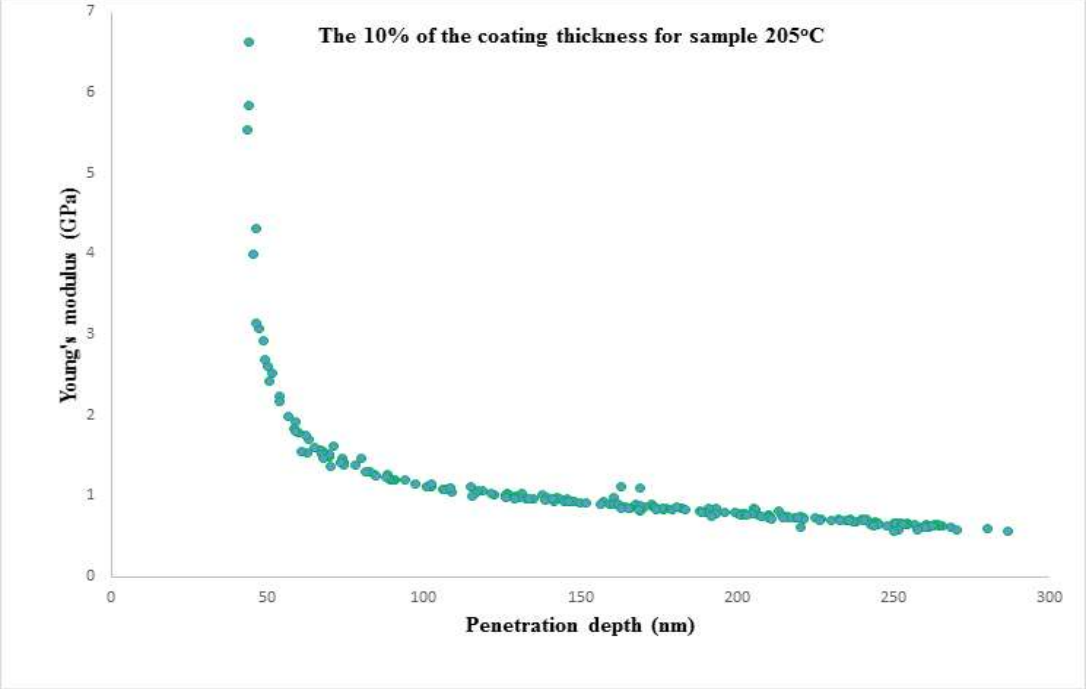

Figure 4. 11: Young's modulus E versus penetration depth hmax relationship for 205ºC blade melting gel specimen. Young's modulus decreases with increased indentation depth.

4.4 Nanoindentation of the 175°C blade coated melting gel thin films on silicon substrate – heat treatment in vacuum

One of the observations made during the post processing of the melting gel specimens involves the oxygen diffusion during the heat treatments. The assumption is that the diffused oxygen strongly reacts with the methyl-roots (organic group) and burns them resulting in a stiff surface skin, i.e., higher H and E values, due to the removal of *O-H* and CH_3 bonds leaving behind a stripped silica network. In order to test this assumption, the 175^0C specimen was treated in vacuum in order to avoid the oxygen effect. The resulting nanoindentation data is presented in Figure 4.12. The peak load for 175^oC vacuum treated melting gel specimen is 1850μN at penetration (indentation) depth of 1331nm. At highest peak load the penetration depth is smaller than the value of 10% film thickness (13600 nm, Table 4.2).

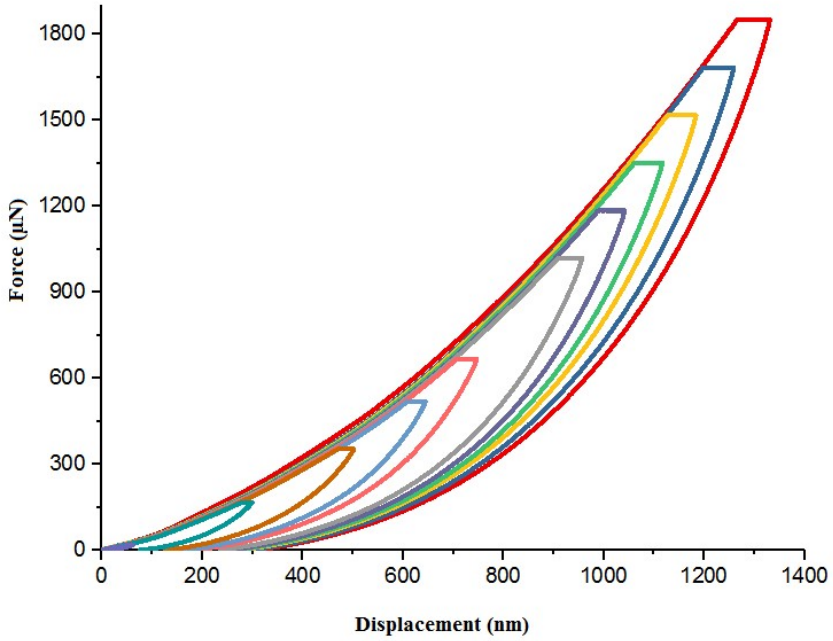

Figure 4. 12: Force versus displacement curves at the peak load for the 175ºC vacuum treated melting gel thin film (maximum depth 1331nm, maximum peak load 1850μN).

The mechanical properties of blade sample heated treated at 175^oC in vacuum are

illustrated in Figures 4.13 and 4.14. Representative hardness and Young's modulus are 0.071GPa, and 0.65GPa, respectively. These values are calculated using a data set of 225 indents (15x15 indentation grid) in the constant range of 1000-1300nm of the coating.

The hardness and Young's modulus of the specimen that was heated to 175^oC in vacuum are consistently lower than the corresponding ones of the non-vacuum specimens. Specifically, the non-vacuum 175^oC specimens shows that *representative* hardness is $H=0.098GPa$ while the vacuum experiments with the same heat treatment the representative hardness is $H=0.071GPa$. Similarly, the representative Young's modulus results are $E=0.881GPa$ and $E=0.65GPa$ for the vacuum and non-vacuum for the 175^0C specimens, respectively. The absence of oxygen diffusion and its resulting stiffening effects are illustrated on surface of the specimen. Also, one can notice the very repetitive indentation curves in Figure 4.12. The data for these curves is taken in different positions on the specimen and their even nature indicates absence of surface modification (hardening, stiffening) due to the lack of oxygen diffusion.

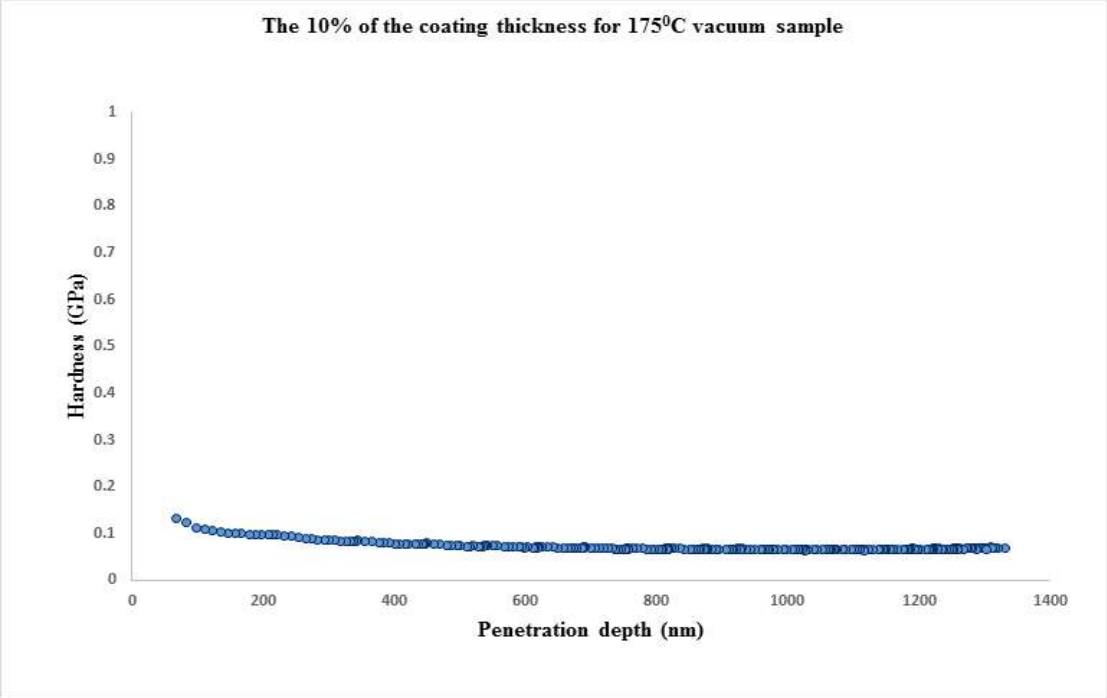

Figure 4. 13: Hardness H versus penetration depth hmax relationship for 175ºC vacuum blade melting gel specimen. Young's modulus decreases with increased indentation depth.

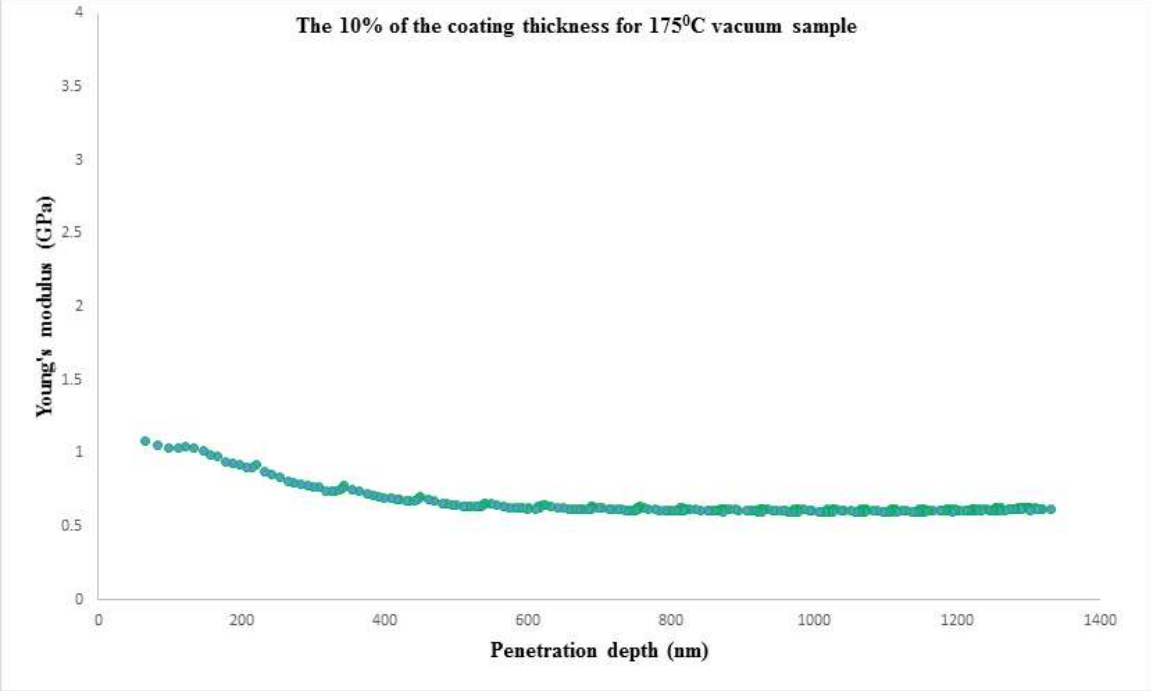

Figure 4. 14: Young's modulus E versus penetration depth hmax relationship for 175ºC vacuum blade melting gel specimen. Young's modulus decreases with increased indentation depth.

Table 4.3 summarizes the results from the experimental characterization of the blade melting gel specimens heat treated at three different temperatures, 145^0C, 175^0C, and 205^0C, and illustrates the effect of the vacuum processing during heat treatment for the 175^0C specimens. It is illustrated that as the heat treatment temperature increases the effects of oxygen diffusion are becoming more prominent.

Table 4. 3: Experimental material properties of the blade melting gel specimens

Sample (Heated Temperature)	Maximum Depth (nm)	Pmax (μN)	Hardness (GPa)	Elastic Modulus (GPa)
145 ^{o}C	1000	1100	0.061	0.735
175 ^{o}C	887	1000	0.098	0.881
175 ^{o}C VACUUM	1331	1850	0.071	0.65
205 ^{o}C	287	95	0.041	0.56

To elaborate, the mechanical properties of the melting gel thin film on the silicon substrate decrease as the penetration depth increases. This is due to the dehydroxilation and deethyoxylation at temperatures higher than 150^0C at which the melting gel starts to consolidate, note that the consolidation temperature for the melting get is 120^0C-170^0C. That effect together with the viscoelastic behavior of the consolidated melting gel (polymer) are responsible for the decrease of the mechanical properties in the bulk of the thin film (compare 145^0C and 175^0C property values in Table 4.3). Getting closer to the

surface there is an oxidation process that takes place due to the oxygen diffusion in the film creating the *O-H*, CH_2 and CH_3 bonds. Up to $\sim 175^oC$ which is a temperature at the higher end of the consolidation range of this material the presence of these bonds creates a stronger skin on the surface of the specimen, resulting in the higher values of hardness and Young's modulus at the film's surface. At higher temperatures the oxygen reacts with the organic roots of the precursors, which will burn (*O-H*, CH_2 and CH_3 bonds are removed) after the consolidation temperature is reached leaving behind a silica network.

It is observed from the melting gel structure that the methyltiethoxysilane and phenyltriethoxysilane precursors play an important role in the melting gel composition and act as network modifiers. Increasing the heat treatment temperature will lead to reduced surface hydroxyl, but this is followed by hydroxylation over the time. Using MTES as a precursor can cause the increase of the CH_3 on the surface during the high heat treatments, which will also improve the mechanical properties on the surface; however, as the penetration depth increases the above effects are halted and the enhancement of the mechanical properties diminishes [56].

Moreover, the thickness of the thin film decreases with increased concentration of DMDES precursor, since DMDES increases the viscosity of the specimen [56, 57]. Kakiuchida et al. have indicated that increasing the number of phenyl group in the precursor will decrease the number of bridging oxygen leaving behind three-dimensional siloxane networks [58]. Consequently, the above-mentioned phenomena act synergistically with the oxygen diffusion and produce a region closer to the surface where the material properties are improved, with the exception of the 205^0C specimen which is heat treated

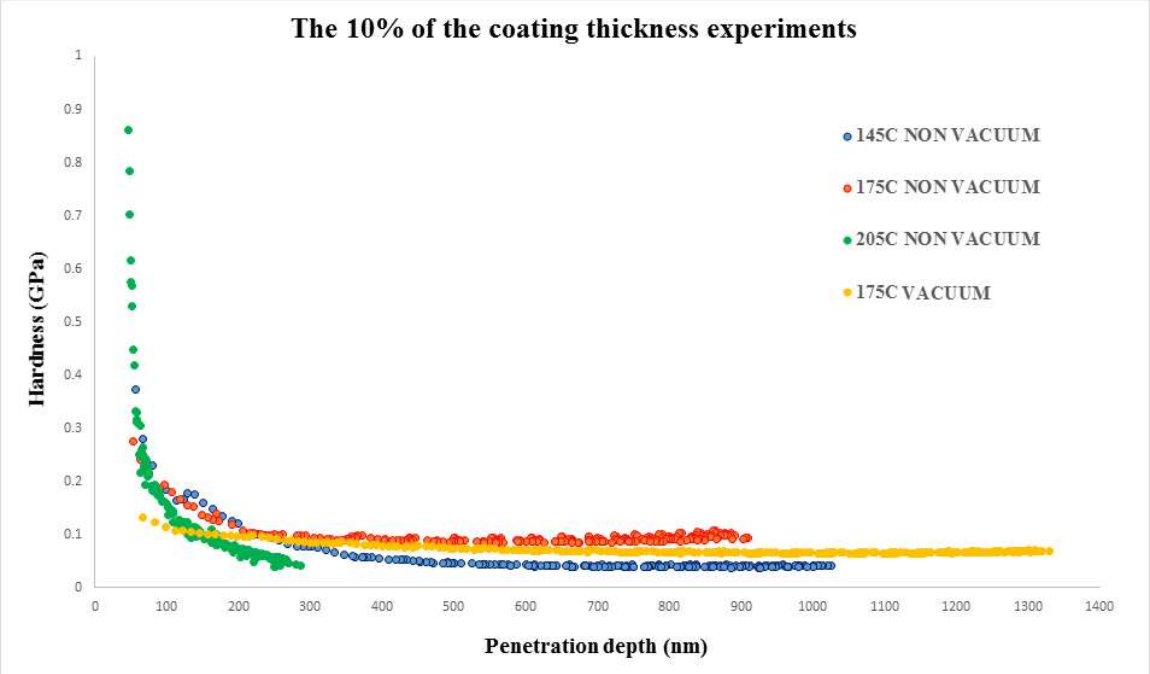

Figure 4. 15: Hardness H versus penetration depth h_{max} for blade melting gel specimens. Hardness decreases with increased indentation depth.

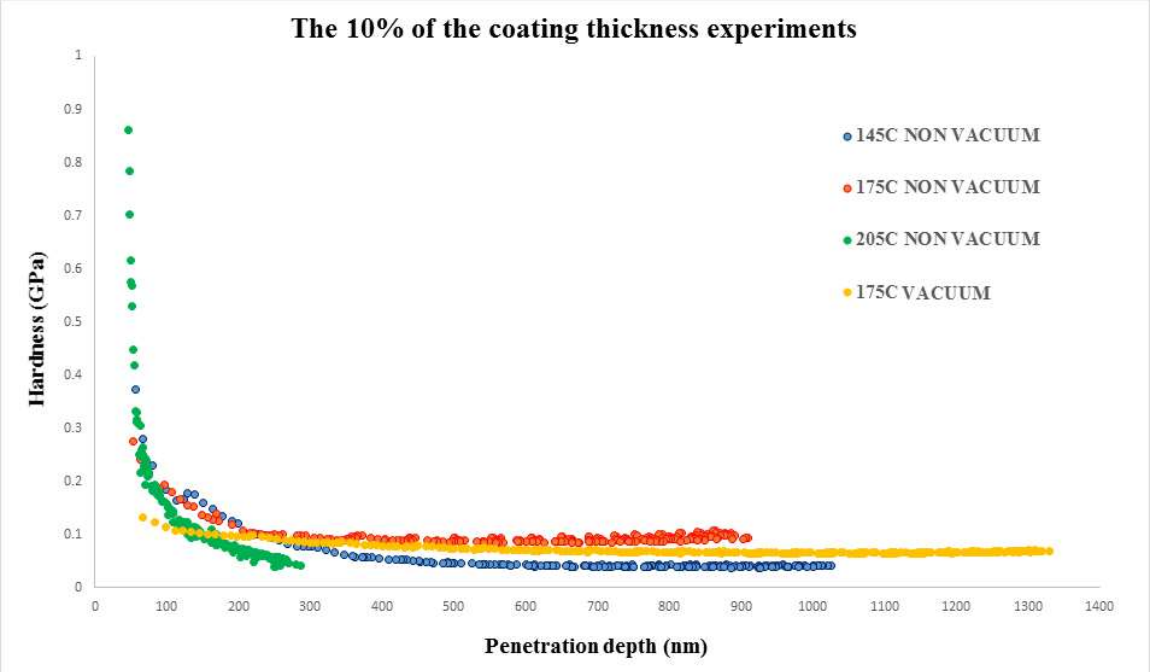

Figure 4. 16: Young's modulus E versus penetration depth h_{max} blade melting gel specimens. Young's modulus decrease with increased indentation depth.

at higher than the consolidation temperature at which the CH_2, CH_3 and OH bonds are burned.

Figures 4.15 and 4.16 illustrate the effect of post processing heat treatment on the melting gel mechanical response. All non-vacuum heat treated specimens illustrate reduction of the mechanical properties with increased indentation depth. The 145^oC specimens exhibit lower mechanical properties than the 175^oC which confirms the discussion above.

The vacuum results show that the mechanical properties remain almost the same with the increasing indentation depth while the non-vacuum results illustrate a clear relationship between the material properties and the depth of indentation. Specifically, in the 175^oC non-vacuum melting gel data the hardness starts at $0.0275GPa$ while for the 175^0C vacuum experiments the hardness onset value is $0.013GPa$. The difference in the hardness is attributed to oxygen reaction creating $O\text{-}H$, CH_2 and CH_3 bonds. In this temperature, the cross-linking is completed because it is close to the consolidation temperature, and the organic group which is methyl and phenyl are starting to burn.

The hardness and the Young's modulus in the vacuum melting gel specimen decreased by 38% and 26%, respectively, compared to the corresponding values of the non-vacuum specimen. The mechanical response through the thickness of the vacuum specimens is more uniform than that of the non-vacuum ones due to the lack of oxygen in the processing environment, resulting in almost constant values of H and E through the thickness of the specimen.

4.5 Displacement control experiments for non-vacuum blade specimens

In order to investigate the mechanical response of the non-vacuum blade specimens at a reference indentation depth, depth displacement control experiments were performed at 288nm (blade melting gel, heat treatment at 205^oC, smallest depth used in our tests). The experimental data illustrate that highest mechanical properties occured with increased heat treatment temperature of the samples. For instance, the value of hardness and Young's modulus for the 145^oC blade samples are $H=0.05GPa$ and $E=0.79GPa$, respectively, and are calculated from the constant range of (*200-250nm*). Similarly, the hardness and Young's modulus for the 175^oC specimens can be evaluated in the constant range of (*230-260nm*) and the results are $H=0.14GPa$ and $E=0.96GPa$. Meanwhile, hardness and Young's modulus for the 205ºC specimen are determined in the constant range of (*230-280nm*) and are found to be $H=0.051GPa$ and $E=0.65GPa$, see Figures 4.17 and 4.18.

Cross-linking and oxygen diffusion took place after the melting gel consolidation process (processing temperature were varied) resulting in deteriorated mechanical properties [23, 56, 59, 60]. Therefore, the hardness of sample 175^oC is higher than the hardness in sample 145^oC by 64.2% since the cross-linking is not completed in the heat treatment and the *O-H*, CH_2 and CH_3 bonds are still intact. While the hardness and Young's modulus values of the 205^oC specimen decrease with the increase in the indentation depth. The oxygen reaction in the high heat treatment significantly alters the specimen's surface, resulting to altered mechanical properties in low indentation depths, ie., close to the surface, see Figure 4.17. Similar results are observed for the Young modulus, see Figure 4.18.

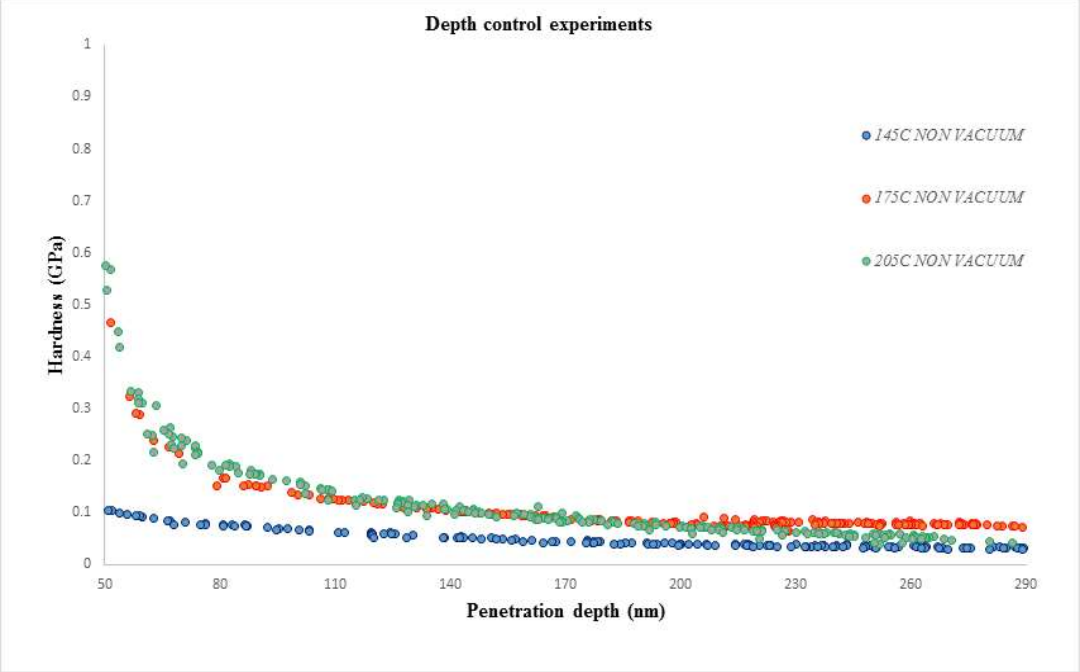

Figure 4. 17: Hardness H versus penetration depth h_{max} for blade, non-vacuum, melting gel specimens. Hardness decreases with increased indentation depth.

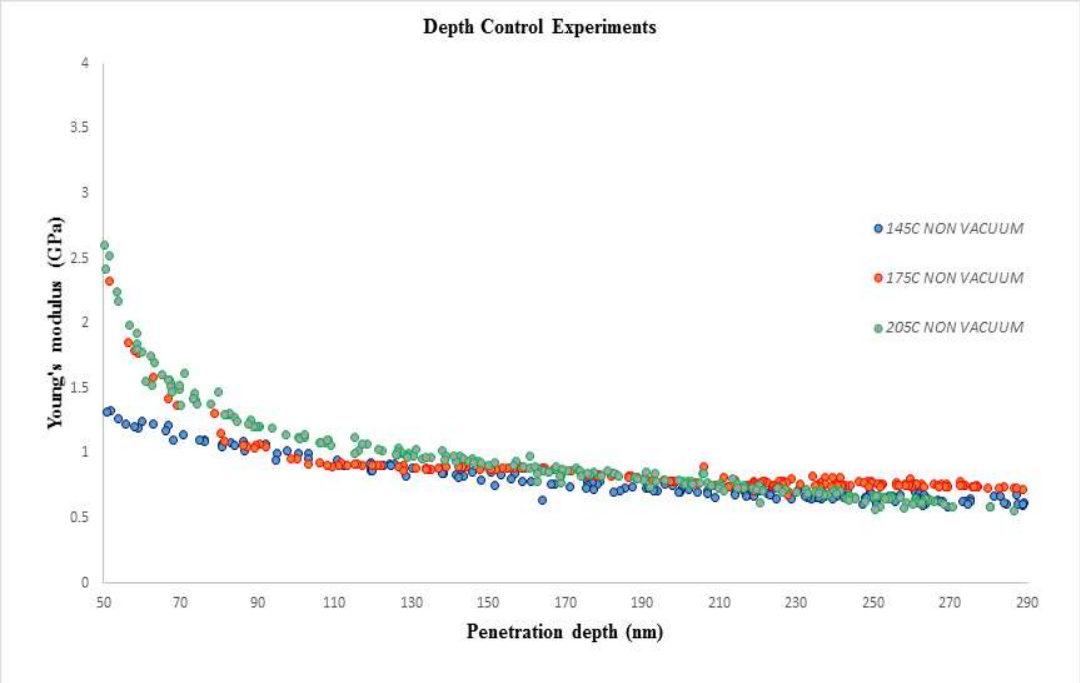

Figure 4. 18: Young's modulus E versus penetration depth h_{max} for blade, non-vacuum, melting gel specimens. Young's modulus decreases with increased indentation depth.

One should notice that in depth controlled experiments the melting gel properties are being probed in the same region from the free surface of the specimens. This eliminates the thickness affect and focuses on the diffusion and chemical reactions happening close to, or on, the surface of the specimens as a function of the post processing temperature. In this depth region, which is limited to 300nm, it is clear that the hardness and the Young's modulus values increase with increasing the temperature of the blade melting gel from 145^0C, to 175^0C and eventually to 205^0C. Apparently, the effect of oxidation on the surface of the specimen plays an important role in creating a thin hard skin on the surface. The dense layer could act as a barrier coating with tuned mechanical properties to prevent delamination, while the sparse or coating layer can act as a superthydrophobic/anti-fouling functional layer.

4.6 Load control experiments for vacuum and non- vacuum specimens

In these experiments, the maximum load required to reach the 10% of the coating thickness for the 205ºC blade vacuum specimen was applied, that load being 95 μN. Therefore, a series of indentations in the range of 30-90μN was conducted for all specimens to test their mechanical response under the same loading conditions. Similarly to the depth control experiments, the mechanical properties of specimens with higher temperature heat treatments are improved. This is because we are probing a very shallow region of the specimens where the oxygen diffusion and oxidation effects are prominent. The mechanical properties decrease with the increasing the force of the indenter which reflects to the viscoelastic nature of polymers. *O-H*, CH_2 and CH_3 bonds gradually decrease, indicating the consolidation process is more complete though the coating thickness. The hardness and Young's modulus values for 145^oC blade, non-vacuum, specimen are *H=0.019GPa* and *E=0.44GPa*, respectively, and are calculated at the constant range of (*60-65μN*). The mechanical properties for 175^oC blade, non-vacuum, specimen are *H=0.18GPa* and *E=0.92GPa* and are evaluated in the constant range of (88-95*μN*). Meanwhile, the mechanical properties for the 205^oC specimen are decreased dramatically to the levels of *H=0.023GPa* and *E=0.089GPa*, with the values determined at constant range of (80-95*μN*), see Figures 4.19, 4.20. This dramatic decrease in the *H* and *E* values of the 205^oC specimen may be attributed to its removed bonds on the specific crosslinking that occurs during consolidation.

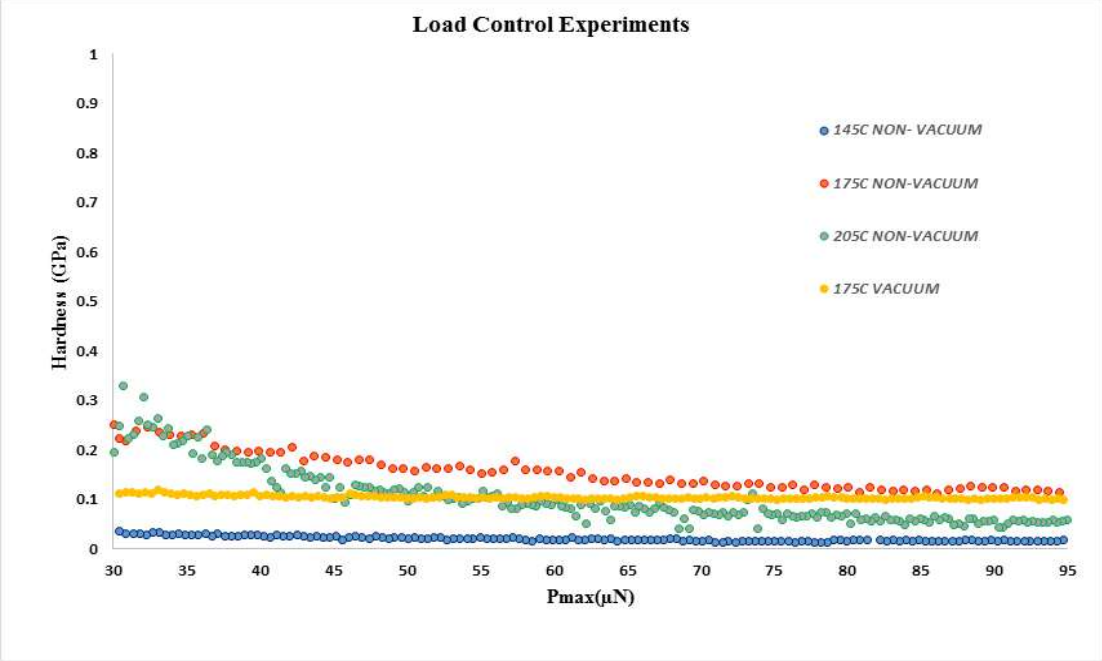

Figure 4. 19: Hardness H versus maximum P_{max} for blade, vacuum and non-vacuum melting gel specimens. Hardness decreases with increased indentation depth.

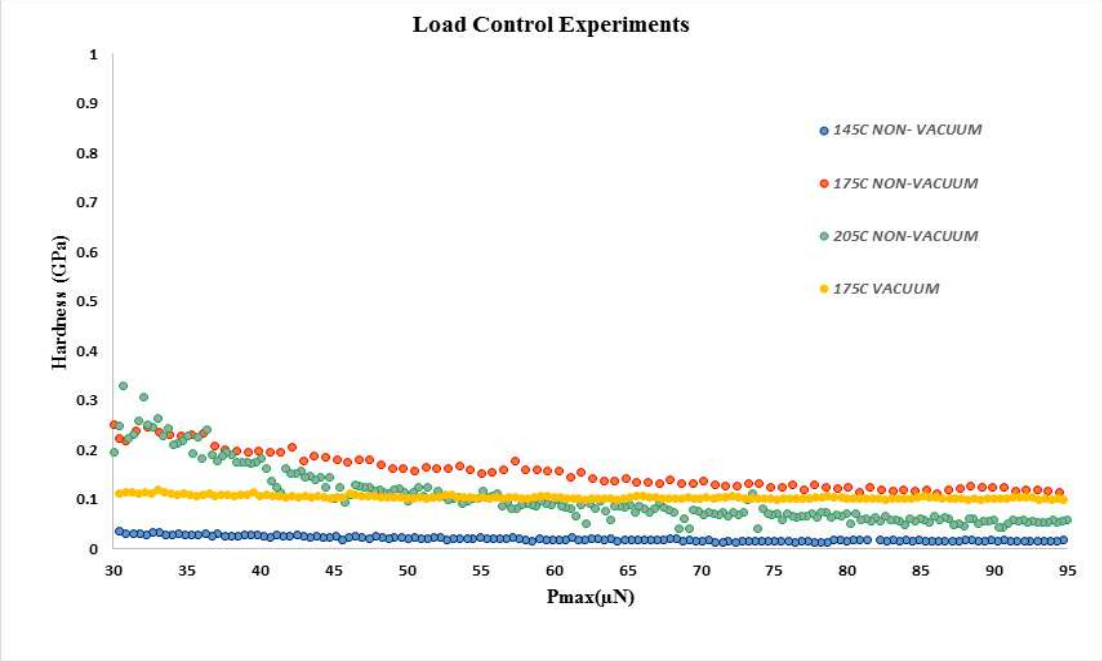

Figure 4. 20: Young's modulus E versus P_{max} for blade, vacuum and non-vacuum, melting gel specimens. Young's modulus decreases with increased indentation depth.

Chapter 5

CONCLUSIONS

In this study, the mechanical characterization of a melting gel (MG) thin film, consisting of methyltriethoxysilane (MTES) and dimethyldiethoxysilane (DMDES) at a molar ratio of 65:35 and with Tc: *150 ℃* ~ 170 *℃,* is processed using blade coating technology and heat treated at three different temperatures, namely 145^0C, 175^0C, and 205^0C. The hardness and Young's modulus of the melting gel thin film are evaluated using a Hysitron TI750 Ubi nanoindenter due to its capability to probe material properties at low loads, i.e., in the range of μN.

The results of the nanoindentation experiments indicate that the hardness and the Young's modulus of the melting gel thin film decreases with increased indentation depth, indicating that the thin film is harder and has higher elastic modulus closer to its free surface. During experimentation certain geometric provisions are accounted to avoid substrate effects from the Si wafer, one such provision requires restricting the indentation depth to less than 10% of the specimen's thickness. With the restriction on indentation depth taken into account the hardness and Young's modulus for the melting gel thin film 145^oC blade specimen are *0.061GPa* and *0.735GPa* (measured within a constant range of 400-900nm of the coating's thickness), the 175^oC blade specimen are *0.098GPa* and *0.881GPa* (measured within a constant range of 300-500nm of the coating's thickness), and the 205^oC blade specimen are *0.041GPa* and *0.56GP (*measured within a constant range of 250-300nm of the coating's thickness), respectively.

From studying the aforementioned results, it should be recognized that in our processing and consolidation phases there are two mechanisms at work. Above ~150^oC,

the melting gel consolidates through dehydroxilation and deethyoxylation, releasing water and ethanol and converting to the hybrid gel and enabling the observed mechanical response (i.e., degradation of the *H* and *E* at deeper indentations) of the MG through most of its thickness. The second process is the oxidation that occurs at the surface of the samples as the organic groups are burnt away at elevated temperatures. This causes the values of *H* and *E* increase near the surface in all specimens, as the *O-H,* CH_2, and CH_3 bonds are removed leaving a stripped silica network.

In order to investigate the effect of oxygen presence during processing we performed studies in vacuum at 175^0C and compared the results with those obtained while performing the experiment at the 175^0C while not in vacuum.". The vacuum specimen exhibited smaller values *H* and *E* compared to the non-vacuum one, the results being *H=0.098GPa* and *E=0.881GPa* for the vacuum and H=*0.071GPa* and *E=0.65GPa* for the non-vacuum environment. Study of these data suggests the significant effect of oxygen on the improvement of the mechanical properties on the surface of the thin films.

In addition, displacement and load control nanoindentation at reference depth and load ranges, calculated from the specimens with the smaller thickness, were performed. These experiments were conducted to further study the oxidation effect on the surface of the specimen. For the displacement control tests, the thinnest specimen used was the 205^0C blade MG and the applicable indentation depths for all three heat treated specimens were in the range of (200-300nm). The results consistently indicate that the 145^0C (*H=0.05GPa* and *E=0.79GPa*), properties are inferior to those of 175^0C (*H=0.14GPa* and *E=0.96GPa*), which is expected since the 175^0C specimen is exposed to higher temperatures where the oxidation effect is more prominent. In contrast, the specimen heat treated at 205^0C is

bounded between the other two values in the nanoindentation depth range of interest (200-300nm). The fact that lower *H* and *E* values were observed in the 205^0C specimen than the 175^0C specimen may be attributed to differences in the specific crosslinking that occurs during consolidation.

The load controlled nanoindentations illustrate the improvement of the mechanical properties at small nanoindentation loads, i.e., 30-90μN, which here translated to small indentation depths, where the oxygen diffusion and oxidation effects are prominent. As expected, the results follow the trends seen in displacement control experimentation.

A more detailed study of the mechanical properties in the bulk of the thin film is necessitated to discern the mechanisms responsible for the inversion of the mechanical properties of the 145^0C and 175^0C blade specimens in the (300-900nm) nanoindentation depth range will be included in future studies. In addition, a comparison of the presented data with experimental results from electrosprayed melting gels should be performed in future, to compare effectiveness of the two MG processing methods.

References

1. Oliver, W.C. and G.M. Pharr, *An improved technique for determining hardness and elastic modulus using load and displacement sensing indentation experiments.* Journal of materials research, 1992. **7**(6): p. 1564-1583.
2. Oliver, W.C. and G.M. Pharr, *Measurement of hardness and elastic modulus by instrumented indentation: Advances in understanding and refinements to methodology.* Journal of materials research, 2004. **19**(1): p. 3-20.
3. Sneddon, I.N., *The relation between load and penetration in the axisymmetric Boussinesq problem for a punch of arbitrary profile.* International journal of engineering science, 1965. **3**(1): p. 47-57.
4. Saha, R. and W.D. Nix, *Effects of the substrate on the determination of thin film mechanical properties by nanoindentation.* Acta Materialia, 2002. **50**(1): p. 23-38.
5. Han, S.M., R. Saha, and W.D. Nix, *Determining hardness of thin films in elastically mismatched film-on-substrate systems using nanoindentation.* Acta Materialia, 2006. **54**(6): p. 1571-1581.
6. Tiwari, A. and S. Natarajan, *Applied Nanoindentation in Advanced Materials*. 2017: John Wiley & Sons.
7. King, R., *Elastic analysis of some punch problems for a layered medium.* International Journal of Solids and Structures, 1987. **23**(12): p. 1657-1664.
8. Roos, J., JP. Celis., E. Vancoille., H. Veltrop and S. Boelens, *Interrelationship between processing, coatingproperties and functional properties of steered arc physically vapour deposited (Ti, AI) N and (Ti, Nb) N coatings.* Thin Solid Films, 1990. **193**: p. 547-556.
9. VanLandingham, M.R. and JS. Villarrubia, *Nanoindentation of polymers: an overview*. in *Macromolecular symposia*. 2001. Wiley-Blackwell, 111 River Street Hoboken NJ 07030-5774 USA.
10. Tang, B., A. Ngan, and J. Pethica, *A method to quantitatively measure the elastic modulus of materials in nanometer scale using atomic force microscopy.* Nanotechnology, 2008. **19**(49): p. 495713.
11. Suresh, S. and A. Giannakopoulos, *A new method for estimating residual stresses by instrumented sharp indentation.* Acta Materialia, 1998. **46**(16): p. 5755-5767.
12. Li, C., F. Zhang., B. Meng and Z Ma, *Simulation and Experiment on Surface Morphology and Mechanical Properties Response in Nano-Indentation of 6H-SiC.* Journal of Materials Engineering and Performance, 2017. **26**(3): p. 1000-1009.
13. Liskiewicz, T., K. Kubiak, and T. Comyn, *Nano-indentation mapping of fretting-induced surface layers.* Tribology International, 2017. **108**: p. 186-193.
14. Fischer-Cripps, A.C., *Introduction to contact mechanics*. 2000: Springer.
15. Chudoba, T. and F. Richter, *Investigation of creep behaviour under load during indentation experiments and its influence on hardness and modulus results.* Surface and Coatings Technology, 2001. **148**(2): p. 191-198.
16. Singh, D., N. Chawla., G. Tang and YL Shen , *Micropillar compression of Al/SiC nanolaminates.* Acta Materialia, 2010. **58**(20): p. 6628-6636.
17. Gao, S., S. Gao., B. Xu and H. Yu, *Effects of different ph-values on the nanomechanical surface properties of peek and cfr-peek compared to dental resin-based materials.* Materials, 2015. **8**(8): p. 4751-4767.

18. Liu, E., H Wang, G. Xiao., G. Yua and X. Shu , *Creep-related micromechanical behavior of zirconia-based ceramics investigated by nanoindentation.* Ceramics International, 2015. **41**(10): p. 12939-12944.
19. Bandyopadhyay, P., D Chicot, CS Kumar, *Influence of sinking-in and piling-up on the mechanical properties determination by indentation: A case study on rolled and DMLS stainless steel.* Materials Science and Engineering: A, 2013. **576**: p. 126-133.
20. Cheng, Y.-T. and C.-M. Cheng, *Scaling relationships in conical indentation in elastic-plastic solids with work-hardening.* MRS Online Proceedings Library Archive, 1998. **522**.
21. Klein, L. and A. Jitianu, *Synthesis of Melting Gels Using Mono-Substituted and Di-Substituted Alkoxysiloxanes.* 2012.
22. Hrubesh, L.W. and J.F. Poco, *Thin aerogel films for optical, thermal, acoustic and electronic applications.* Journal of non-crystalline solids, 1995. **188**(1-2): p. 46-53.
23. Jitianu, A., G. Amatucci, and L.C. Klein, *Phenyl-Substituted Siloxane Hybrid Gels that Soften Below 140° C.* Journal of the American Ceramic Society, 2009. **92**(1): p. 36-40.
24. Jitianu, A. and L. Klein, *Encapsulating Battery Components with Melting Gels.* Ceramic Transactions, Advances in Materials Science for Environmental and Energy Technologies III, ed. T. Ohji, J. Matyas, NJ Manjooran, G. Pickrell and A. Jitianu, American Ceramic Soc., Westerville, OH, 2014. **250**: p. 279-286.
25. Hösel, M., *Large-scale roll-to-roll fabrication of organic solar cells for energy production*. 2013: Department of Energy Conversion and Storage, Technical University of Denmark.
26. McElhaney, K., J. Vlassak, and W. Nix, *Determination of indenter tip geometry and indentation contact area for depth-sensing indentation experiments.* Journal of Materials Research, 1998. **13**(5): p. 1300-1306.
27. Veprek-Heijman, M.G., *Measurements of Hardness and Other Mechanical Properties of Hard and Superhard Materials and Coatings*, in *Microstructure-Property Correlations for Hard, Superhard, and Ultrahard Materials*. 2016, Springer. p. 105-134.
28. Gaskell, S.J., *Electrospray: principles and practice.* Journal of mass spectrometry, 1997. **32**(7): p. 677-688.
29. Chen, J. and S. Bull, *On the factors affecting the critical indenter penetration for measurement of coating hardness.* Vacuum, 2009. **83**(6): p. 911-920.
30. Roa, J., E. Gilioli., F Bissoli., F. Pattini and S. Rampino, *Study of the mechanical properties of CeO 2 layers with the nanoindentation technique.* Thin Solid Films, 2009. **518**(1): p. 227-232.
31. Sakai, M., J. Zhang, and A. Matsuda, *Elastic deformation of coating/substrate composites in axisymmetric indentation.* Journal of materials research, 2005. **20**(8): p. 2173-2183.
32. Huajian, G., C. Cheng-Hsin, and L. Jin, *Elastic contact versus indentation modeling of multi-layered materials.* International journal of Solids and Structures, 1992. **29**(20): p. 2471-2492.
33. Song, H., *Selected mechanical problems in load-and depth-sensing indentation testing*. 1999, Rice University.

34. Xu, H. and G. Pharr, *An improved relation for the effective elastic compliance of a film/substrate system during indentation by a flat cylindrical punch.* Scripta Materialia, 2006. **55**(4): p. 315-318.
35. Rar, A., H. Song, and G. Pharr, *Assessment of new relation for the elastic compliance of a film-substrate system.* MRS Online Proceedings Library Archive, 2001. **695**.
36. Hay, J. and B. Crawford, *Measuring substrate-independent modulus of thin films.* Journal of Materials Research, 2011. **26**(6): p. 727-738.
37. Simmons, G. and H. Wang, *Single crystal elastic constants and calculated aggregate properties.* 1971.
38. Huang, X. and A.A. Pelegri, *Nanoindentation measurements on low-k porous silica thin films spin coated on silicon substrates.* TRANSACTIONS-AMERICAN SOCIETY OF MECHANICAL ENGINEERS JOURNAL OF ENGINEERING MATERIALS AND TECHNOLOGY, 2003. **125**(4): p. 361-367.
39. Jee, A.-Y. and M. Lee, *Comparative analysis on the nanoindentation of polymers using atomic force microscopy.* Polymer Testing, 2010. **29**(1): p. 95-99.
40. Stafford, C.M., C. Harrison., KL. Beers., A. Karim and EJ Amis, *A buckling-based metrology for measuring the elastic moduli of polymeric thin films.* Nature materials, 2004. **3**(8): p. 545-550.
41. Odegard, G., T. Gates, and H. Herring, *Characterization of viscoelastic properties of polymeric materials through nanoindentation.* Experimental Mechanics, 2005. **45**(2): p. 130-136.
42. Lee, S.-H., S. Wang., GM. Pharr and H Xu, *Evaluation of interphase properties in a cellulose fiber-reinforced polypropylene composite by nanoindentation and finite element analysis.* Composites Part A: Applied Science and Manufacturing, 2007. **38**(6): p. 1517-1524.
43. Richard, A., *Interface and surface effects on the glass-transition temperature in thin polymer films.* Faraday Discussions, 1994. **98**: p. 219-230.
44. Huang, J., PF. Miller and JS. Wilson, *Investigation of the effects of doping and post-deposition treatments on the conductivity, morphology, and work function of poly (3, 4-ethylenedioxythiophene)/poly (styrene sulfonate) films.* Advanced Functional Materials, 2005. **15**(2): p. 290-296.
45. Yang, D., A. Velamakann., G. Bozoklu., S. Park, and M. Stoller,, *Chemical analysis of graphene oxide films after heat and chemical treatments by X-ray photoelectron and Micro-Raman spectroscopy.* Carbon, 2009. **47**(1): p. 145-152.
46. Petersen, K.E., *Silicon as a mechanical material.* Proceedings of the IEEE, 1982. **70**(5): p. 420-457.
47. Huang, R., M. Sone.,W. Ma, and H. Fukanuma, *The effects of heat treatment on the mechanical properties of cold-sprayed coatings.* Surface and Coatings Technology, 2015. **261**: p. 278-288.
48. Peresin, M.S., K Kammiovirta and H Heikkinen, *Understanding the mechanisms of oxygen diffusion through surface functionalized nanocellulose films.* Carbohydrate polymers, 2017. **174**: p. 309-317.
49. Inoue, G. and M. Kawase, *Effect of porous structure of catalyst layer on effective oxygen diffusion coefficient in polymer electrolyte fuel cell.* Journal of Power Sources, 2016. **327**: p. 1-10.

50. Klinger, M., LP. Tolbod, and KV. Gothelf, *Effect of polymer cross-links on oxygen diffusion in glassy PMMA films.* ACS applied materials & interfaces, 2009. **1**(3): p. 661-667.
51. Shoaee, S. and J.R. Durrant, *Oxygen diffusion dynamics in organic semiconductor films.* Journal of Materials Chemistry C, 2015. **3**(39): p. 10079-10084.
52. Brook, R., *Sol-gel technology for thin films, fibers, preforms, electronics and specialty shapes. Edited by LC Klein. Noyes Publications, New Jersey, USA 1988. xxi, 407 pp., bound, US $72.–ISBN 0-8155-1154-X.* Advanced Materials, 1989. **1**(8-9): p. 309-309.
53. Jitianu, A., G. Gonzalez, and L.C. Klein, *Hybrid Sol–Gel Glasses with Glass-Transition Temperatures Below Room Temperature.* Journal of the American Ceramic Society, 2015. **98**(12): p. 3673-3679.
54. Pharr, G. and W. Oliver, *Measurement of thin film mechanical properties using nanoindentation.* Mrs Bulletin, 1992. **17**(7): p. 28-33.
55. Chen, X. and J.J. Vlassak, *Numerical study on the measurement of thin film mechanical properties by means of nanoindentation.* Journal of Materials Research, 2001. **16**(10): p. 2974-2982.
56. Jitianu, A., J. Doyle., G. Amatucci and LC. Klein, *Methyl modified siloxane melting gels for hydrophobic films.* Journal of sol-gel science and technology, 2010. **53**(2): p. 272-279.
57. Jitianu, A., K. Lammers., A. Arbuckle-Kiel, and L.C. Klein, *Thermal analysis of organically modified siloxane melting gels.* Journal of thermal analysis and calorimetry, 2011. **107**(3): p. 1039-1045.
58. Kakiuchida, H., M. Takahashi, and Y. Tokuda, *Viscoelastic and structural properties of a phenyl-modified polysiloxane system with a three-dimensional structure.* The Journal of Physical Chemistry B, 2006. **110**(14): p. 7321-7327.
59. Sperling, L. and J. Fay, *Factors which affect the glass transition and damping capability of polymers.* Polymers for Advanced Technologies, 1991. **2**(1): p. 49-56.
60. Polyakova, A., RYF Liu, DA Schiraldi, *Oxygen-barrier properties of copolymers based on ethylene terephthalate.* Journal of Polymer Science Part B: Polymerp Physics, 2001. **39**(16): p. 1889-1899.